Field Crops Research 338 (2026) 110311

Contents lists available at ScienceDirect

Field Crops Research

journal homepage: www.elsevier.com/locate/fcr

Utilizing soil characteristics and hybrid machine learning for interpretable potato yield prediction: A study with satin-bowerbird optimization and deep neural network

Masoud Karbasi [a], Gurjit S. Randhawa [b,*], Aitazaz A. Farooque [a,c,**], Mumtaz Ali [d], Mehdi Jamei [a,e], Khabat Khosravi [f], Hassan Afzal [c], Anurag Malik [g], Qamar U. Zaman [h]

[a] Canadian Centre for Climate Change and Adaptation, University of Prince Edward Island, St Peters Bay, PE, Canada
[b] School of Computer Science, University of Guelph, Guelph, ON, Canada
[c] Faculty of Sustainable Design Engineering, University of Prince Edward Island, Charlottetown, PE, Canada
[d] School of Business, Law, Humanities, and Pathways, University of Southern Queensland, QLD 4305, Australia
[e] Faculty of Civil Engineering and Architecture, Shahid Chamran University of Ahvaz, Ahvaz, Iran
[f] Department of Natural Resources, College of Agriculture and Natural Resources, Razi University, Kermanshah, Iran
[g] Punjab Agricultural University, Regional Research Station, Bathinda, Punjab, India
[h] Department of Engineering, Faculty of Agriculture, Dalhousie University, Truro, NS, Canada

ARTICLE INFO

Keywords:
Potato yield
Machine Learning
Deep Learning
Optimization
SHAP

ABSTRACT

Context: Yield forecasting is crucial to the agricultural planning enterprise, such as input control, farm logistics and reduction of economic risks. The soils in the Maritime provinces of Canada have a great difference in their properties which affect the productivity of crops. Such variability requires a strong prediction model that could address the different characteristics of soil.

Objective: This research proposal is expected to establish a stable potato yield prediction model based on the soil property data of New Brunswick and Prince Edward Island and determine whether the application of optimization techniques with deep learning can enhance the prediction accuracy over the conventional machine learning approach.

Methods: Soil samples were taken at eight experimental sites in the 2017 and 2018 growing seasons, with 18 soil properties being captured. The feature selection techniques were used to create three input scenarios (Comb1, Comb2, Comb3). To optimize the selection of input variables, a hybrid prediction model, DNN-SBO (Deep Neural Network -Satin Bowerbird Optimization), was suggested and refined with the Boruta feature selection and Best Subset Regression-WASPAS. The performance of the model was tested in comparison with Kernel Ridge Regression (KRR), Elastic Net, K-Nearest Neighbors (KNN) and Support Vector Regression (SVR), on the evaluation metrics of Correlation Coefficient (R), Root Mean Square Error (RMSE) and Mean Absolute Percentage Error (MAPE). The model interpretability was done using SHAP (Shapley Additive exPlanation) analysis.

Results and Conclusions: Comb2 was the best input scenario that consisted of Total Base Saturation, Sulfur, Magnesium, Potash, Aluminum, Zinc, Phosphate, Manganese, Organic Matter, Iron, and Copper. DNN-SBO model had the best predictive power with R= 0.903 (train) and RMSE= 4.165 t/ha and MAPE= 6.766 % and R= 0.853 (test) and RMSE= 5.522 t/ha and MAPE= 9.707 %. The SHAP analysis has shown that Iron was the most significant predictor (mean SHAP = +5.49), next was Copper, Zinc, Phosphorus, and Organic Matter.

Significance: The paper sheds light on the promise of deep learning that is based on bio-inspired optimization and feature selection techniques in order to achieve a significant increase in crop yield prediction. The findings can lead to the wider use of the similar methods in precision agriculture, which will result in smarter and data-driven farming in variably soiled areas.

* Corresponding author.
** Corresponding author at: Canadian Centre for Climate Change and Adaptation, University of Prince Edward Island, St Peters Bay, PE, Canada
E-mail addresses: randhawg@uoguelph.ca (G.S. Randhawa), afarooque@upei.ca (A.A. Farooque).

https://doi.org/10.1016/j.fcr.2025.110311
Received 28 July 2025; Received in revised form 30 October 2025; Accepted 16 December 2025
Available online 23 December 2025

1. Introduction

Global economic expansion and food safety rely heavily on agricultural production, which forms the basis for the prosperity and progress of communities everywhere. The world's population has been expanding dramatically since the mid-1920s, reaching 8.1 billion in 2024 (www.worldometers.info), yet 820 million people still face food insecurity (Organization, 2021). To address this crisis, the UN's Sustainable Development Goals target hunger eradication, food security, and sustainable agriculture by 2030 (Muruganantham et al., 2022). With projections of 9.7 billion people by 2050, meeting escalating food demands without compromising natural resources has become an unprecedented global challenge. As a result, global food demand is projected to rise significantly, leading to increased competition for fertile land and water resources necessary for agricultural production (Lotze-Campen et al., 2008) . Rijsberman and Molden (2001) emphasize the importance of boosting overall food output by about 40 % while lowering water resources utilized in agriculture by 10–20 % (Rijsberman and Molden, 2001). However, these objectives must be met in light of the projected consequences of climate change, which may have a detrimental influence on crop output and other critical agricultural resources such as water availability. Additionally, other critical resources for food production, including land, fossil energy, and nutrients, are being consumed at rates that exceed their global regeneration capacity (Bindraban et al., 2012; Conijn et al., 2018). Consequently, optimizing crop yields is essential to efficiently utilize limited resources, including fertilizers, water, and land. This guarantees the stability of market dynamics and the consistent production of food (Jayne and Sanchez, 2021).

Potato, the third crop eaten in the world after wheat and rice, is one of the basic species of cultivated crops in the world, particularly on Prince Edward Island (PEI) and New Brunswick (NB) in Canada. Tillage improves the structure of the soil, distribution of residue and organic matter affecting soil biology. Although plowing is reduced to reduce costs and erosion, biodiversity is also reduced, and there is a risk of degradation, which is increased (Roger-Estrade et al., 2000) . Potatoes can grow in a variety of climatic conditions and soils, and it is of value to the food stores of the world. Nonetheless, potatoes cannot tolerate water stress and nutrient deficits so specific irrigation and fertilizer application are required to guarantee the high growth and yield. The weakness of the potato plant to the physical condition of the soil, however, implies that the low tillage will adversely impact the tuber yield.

Historically, the forecasting of crop yield is based on large amounts of historical data and agronomist knowledge. These traditional approaches usually use simple statistical tests or linear regressions. Although they can be relatively applicable in the long-term and stable situation, they have failed to explain the interplay of factors that are complex in contemporary agriculture (Paudel et al., 2021). Machine learning (ML) and deep learning (DL) algorithms can significantly increase the accuracy of prediction of potato yield and cultivation strategies. These predictive models can be improved using data of satellite and drones, soil and weather sensors (rainfall and soil nature and moisture level), farm management data, and plant condition indicators to make the output more practical. Finally, this approach will improve the productivity and sustainability of potato production through the use of more efficient resources and sustainability, as well as yields (Cao et al., 2021a, 2021b; Van Klompenburg et al., 2020).

Artificial Neural Network (ANN) is one of the most widely used models and is increasingly used to address various agricultural challenges. Mishra et al., (2023) examined and predicted the potato production of eight major South Asian nations and the projection was carried out between the years 1961–2028. Their validation outcomes proved that state space and ARIMA models are more effective, which means that XGBoost will have to be refined in this situation. El-Kenawy et al., (2024) used the gated recurrent units (GRUs), K-nearest neighbor (KNN), XGBoost, graph neural networks (GNNs), gradient boosting, ANN, and long short-term memory networks (LSTM) in Predicting Potato Crop Yield. They disclosed that GNNs and LSTMs are more accurate. Tamayo-Vera et al. (2024) examined machine learning models applied to predict the potato yield in Prince Edward Island, Canada, and these models managed to capture the temporal dependence effectively and thus, they greatly enhanced the accuracy of the forecast. Projections indicate potential yield reductions of up to 70 % by 2100 under high-emission scenarios, underscoring the urgent requirement for adaptive agricultural practices and greenhouse gas reduction strategies (Tamayo-Vera et al., 2024). The study by Tamayo-Vera et al. (2025) carried out different ML models in determining the regional potato yields in Prince Edward Island, Canada, such as tree-based, linear-based and ensemble-based models. They determined that the tree-based Random Forest (RF) model was better compared to the other models (Tamayo-Vera et al., 2025). This area of research has been connected to many ML/DL models, which have been evaluated on the basis of their predictive performance (according to the literature review). Thus, it is hard to choose the right, strong and credible models especially to predict crop yield. Moreover, it is worth mentioning that identifying the value of the hyperparameter of the model is not the easiest task and efficient in terms of predicting the modeling. In addition, identifying the optimal input situation and the use of relevant input variables can render the modeling prediction results to be reliable and practical, which has not been studied very much.

The research utilizes the Boruta method and Best Subset Regression (BSR) combined with weighted aggregated sum product assessment (WASPAS) feature selection methods to find key soil properties affecting potato output, leading to better model performance through relevance-based variable selection. The novelty of the current study is the development of several state-of-the-art hybrid modeling frameworks integrated with a new metaheuristic algorithm of Satin Bowerbird Optimizer (SBO) for potato yield prediction for the first time. The main aims of the present study are: (1) predict potato yield prediction at Canadian Maritime Provinces, (2) focus on only soil properties as an input, (3) identify the impact of input variables on the results of machine learning models and find the optimum input combination by Boruta Feature Selection and Best Subset Regression Feature Selection techniques (4) apply WASPAS framework for solving multi-criteria group decision-making (MCGDM) problems (5) compare the prediction accuracy of different ML/DL models including Deep Neural Network (DNN), KNN, SVR, Kernel Ridge Regression (KRR), and Elastic Net optimized with SBO metaheuristic algorithm, and (6) make the results explainable by applying SHAP technique. The proposed research uses SHAP values to explain models while maintaining explainability because stakeholders need to see the effects of soil properties on yield predictions for successful agricultural choices. To the best of the author's knowledge, this is the pioneering effort to employ new hybrid machine-learning models while incorporating a comprehensive set of soil properties as input for yield prediction.

Accurate yield prediction is vital for potato farmers, especially in the Maritime provinces of Canada, where soil and climate variability impact production. It enables better resource management, harvest planning, and reduces financial risk. The proposed DNN-SBO model provides highly accurate forecasts, supporting precision agriculture and sustainable farming practices.

2. Materials and methods

The experimental design, data sources, and analytical techniques employed in this investigation are all covered in this section. The study area and soil data collection protocol are described in Section 2–1. The feature selection framework for identifying pertinent soil variables is explained in Sections 2–2. The Deep Neural Network integrated with Satin Bowerbird Optimization (DNN-SBO) architecture and optimization are presented in Sections 2–3, 2–4, and 2–5. Lastly, the evaluation metrics (Sections 2–7) and explainability techniques (Sections 2–6) are

described to evaluate model performance and interpret soil variable contributions.

2.1. Study area and data

2.1.1. Experimental sites

Eight unique experimental locations were selected in two provinces of the Atlantic region, namely New Brunswick and Prince Edward Island, during the 2017–2018 growing season (Fig. S1 Supplementary Material). A total of 8 sites were sampled (5 sites in Prince Edward Island province and three sites in New Brunswick province). Prince Edward Island province is one of the largest potato producers in Canada, and the Woodstock and Grand Falls regions are also among the most important potato production areas in New Brunswick province. The coordinates and elevation of the sampling points are presented in Fig. S1.

Potato plantings were cultivated and meticulously sampled using a grid system in each experimental location, which covered an area of about 4–5 ha. The fields were partitioned into 36–40 distinct sampling sites, each measuring 30 by 30 m, using a Differential Global Positioning System furnished by Topcon Positioning System Inc., a company located in Livermore, USA. This enabled the systematic collection of physico-chemical, sensor, and soil data. Data was collected four times during the growing seasons in 2017 and 2018. The initial data capture occurred in early June, immediately preceding the germination of the seedlings. The subsequent sampling was conducted in late July, coinciding with the 60-day growth stage of the potato crop. Data collection was guaranteed throughout the entire growing season by conducting the third and fourth samplings in August and September, respectively.

2.1.2. Soil data

Soil chemical properties were examined by the Prince Edward Island Analytical Laboratories (PEIAL) with established and standardized methodologies. The soil organic matter was determined using the loss on ignition method, for which the PEIAL used a muffle furnace (Model 550 Isotemp Series, Fisher Scientific, Pittsburgh, PA, USA) (Schulte and Hopkins, 1996), using the standard methods and protocols [https://www.princeedwardisland.ca/en/information/agriculture/pei-analytical-laboratories-peial]. Phosphorus was measured using the Olsen method (Bowman et al., 1978), K using the Flame photometric method (Mayer and Starkey, 1977), Fe with the colorimetric method (Wilson, 1960), CEC with BaCl2- compulsive exchange procedure (Hendershot and Duquette, 1986), and soil pH was determined using PC titrate. The Lime Index was determined by mixing the SMP buffer solution with soil and measuring its pH (Brown and Cisco, 1984). Other soil nutrients, including Ca, Mg, Zn, Cu, S, and P/Al, were analyzed using inductively coupled plasma optical emission spectroscopy (ICP-OES 6500; Thermo Fisher, Santa Clara, CA, USA). Base saturation was determined using the extraction method devised by PEIAL.

2.1.3. Potato tuber yield data

In each year of the study, during the potato harvest season in October, the yield of tubers was ascertained from every designated grid. A strip measuring three meters in length was demarcated within each grid to collect samples of potato tubers. The soil within this strip was manually excavated to gather the tubers. Following collection, the tubers were placed into individual plastic buckets for the purpose of weighing. The weight of the tubers, recorded in kilograms, was determined using a digital field balance. After the weighing procedure was completed, the potatoes were gently returned to the soil, enabling the farmer to proceed with their harvest. Table S1 shows descriptive statistics on soil properties and yield values (Mean, Standard Deviation, Skewness, Kurtosis, and Quartiles). Also, the histograms and distribution of the used variables are shown in Fig. S2. Table S1 and Fig. S2 show that yield values (target variable) have a near-normal distribution. Some input variables have near-normal distributions, such as pH, Phosphate, Calcium, Boron, Manganese, Aluminum, Lime Index, CEC, and Total Base Saturation. Because the data range has different scales, in order to unify the data, all data were normalized in the range of 0–1 using the relationship.

$$Z_i = \frac{x_i - x_{\min}}{x_{\max} - x_{\min}} \tag{1}$$

Fig. S3 shows the normalized box plots of the used data. According to Fig. S3, the distribution of normalized data can be seen, and the near values of the mean and median values of each variable show that the variables are near normal distribution. The isolation forest method was used to detect the outlier data, consisting of five samples excluded from the database.

In order to investigate the relationship between input and target variables, the Pearson correlation values are shown in a correlogram in Fig. 1. The correlation between yield and various soil parameters reveals significant insights: Manganese shows a strong positive correlation of 0.47, indicating its beneficial impact on yield, followed by zinc at 0.4. In contrast, Aluminum and pH present moderate negative correlations at −0.38 and −0.19, respectively, suggesting they detrimentally affect productivity. Other variables, such as Calcium (0.05), P/Al (0.15), and Organic Matter (0.20), exhibit weak to moderate positive correlations, while the Lime Index (-0.05) and Sodium (-0.08) show weak negative relationships. However, these correlation values only indicate the linear relationship between variables and cannot uncover nonlinear relationships in most natural phenomena.

2.2. Feature selection

2.2.1. Boruta feature selection

The Boruta method is a general selection technique that selects variables by comparing the significance of the original features to random queries (Kursa and Rudnicki, 2010). The Boruta package, a well-liked wrapper feature selection technique, extends the random forest classification algorithm. Recently, it has been used in hybrid machine-learning models that may be applied to engineering issues (Jamei et al., 2024; Karbasi et al., 2024). The feature importance is evaluated numerically using the random forest classification technique, which may be used with the default settings. This algorithm's main goal is to add more randomization to the original system and mix it with it to investigate the importance of the features used in the regression and classification investigations.

2.2.2. Best subset regression feature selection

BSR is the model choice procedure that uses statistical terms to choose the best model after assessing all the possible combinations of predictor variables during the initial preprocessing stage (Jović et al., 2015). The process of BSR may be described in the following way: Test all possible models with a maximum of k variables that include one, two or more. The most suitable model of size k is then selected and models of size one and two are selected. The model that has the most overall quality is selected among the finalists.

The optimum subset selection selects one model among a number of 2^k possible models. Statistical rules like the coefficient of Mallow (Cp) (Kobayashi and Sakata, 1990), mean square error (MSE), adjusted R^2_{adj}, Akaike Information criterion (AIC) (Akaike, 1974) and determination coefficient (R 2) were adopted to maximize the subset selection. Adjusted R 2, the information formulae of Akaik and the mallow are defined as:

$$C_p = \frac{RSS_k}{MSE_J} + 2M - N \tag{2}$$

$$AIC = 2k + N.\ln\left(\frac{1}{N}\sum_{i=1}^{N} e_i^2\right) \tag{3}$$

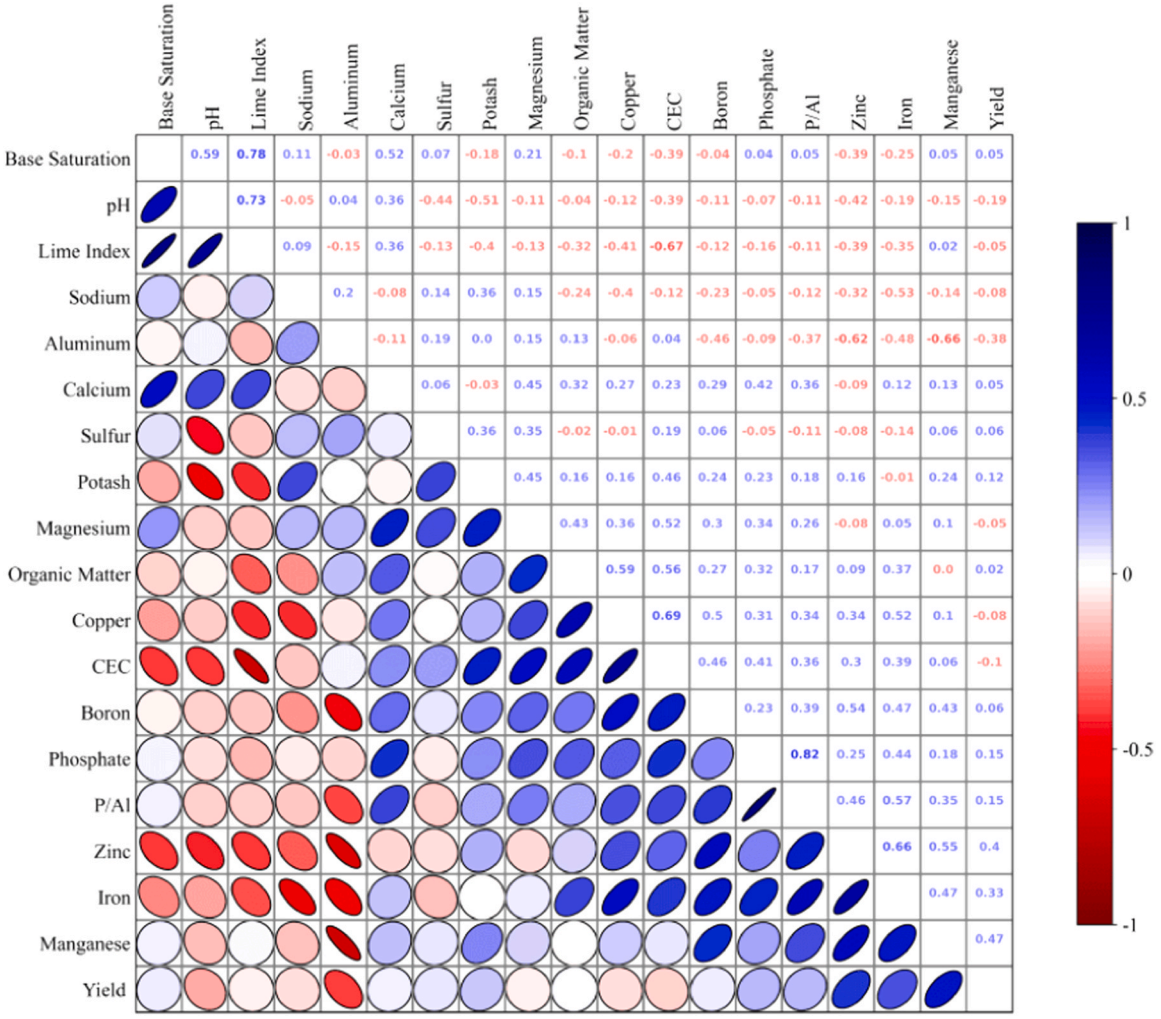

Fig. 1. Correlation between variables.

$$AdjustedR^2 = 1 - \frac{(1-R^2)(N-1)}{N-M-1} \tag{4}$$

$$MSE = \frac{1}{N}\sum_{i=1}^{N} e_i^2 \tag{5}$$

Where M denotes the total number of variables, N represents the sample size, and MSE_J signifies the mean square error. The residual sum of squares is symbolized as RSS_k, represents the sum of the squared residuals obtained from regression models and e_i is the ith residual value.

2.2.3. WASPAS MCDM (Weighted aggregated sum product assessment)

In many real world situations, we often find the conflicting behavior of decision-experts (DEs) about their preferences based on their level of knowledge, settings as well as expertise concerning the alternatives. One of the most common tools that can be used to deal with such problems is multi-criteria decision-making (MCDM) issues (Mishra et al., 2019). One of the efficient methods of MCDM is called the Weighted Aggregated Sum Product Assessment (WASPAS) (Zavadskas et al., 2012). The rapid development and such wide application of this approach can be associated with the simplicity of its calculation, providing rather close results when comparing and selecting some solutions in comparison with rival criteria. The next steps outline the mathematical way the WASPAS technique works (Debnath et al., 2023).

1- The criteria (C_j) and alternative (A_i) are selected for evaluation during the initial phase. Given the set $i = 1, 2, \ldots, m$ and $j = 1, 2, \ldots, n$.

2- In the second phase, the weights of the criteria are determined using one of the MCDM methodologies. Stepwise weight assessment ratio analysis (SWARA) was employed to quantify the weights of the criteria in this investigation.

3- Eqs. (6) and (7) are implemented in Step 3 to normalize the decision matrix. In order to maximize the beneficiary,

$$\overline{X}_{ij} = X_{ij}/\max X_{ij} \tag{6}$$

For the minimum optimum value

$$\overline{X}_{ij} = \min X_{ij}/X_{ij} \tag{7}$$

4- The initial total relative significance value $\left(Q_i^{(1)}\right)$ can be computed utilizing Eq. (8) using the "Weighted Sum Model" in the fourth stage.

$$Q_i^{(1)} = \sum_{j=1}^{n} \overline{X}_{ij} W_j \tag{8}$$

5- Eq. (9) is employed to calculate the second total relative significance value $(Q_i^{(2)})$ in Step 5, where the "Weighted Product Model (WPM)" is executed.

$$Q_i^{(2)} = \prod_{j=1}^{n} \left(\overline{X}_{ij}\right)^{W_j} \tag{9}$$

6- Eq. (10) is employed to calculate the aggregate total relative significance value (Q) in Step 6, where λ denotes the coefficient value of Q.

$$Q_i = \lambda Q_i^{(1)} + (1-\lambda) Q_i^{(2)} \tag{10}$$

2.2.4. Integration of the two-stage feature selection framework

In the research, the combination of Boruta, Best Subset Regression (BSR), and WASPAS was employed to complement in two-stage feature selection frameworks to minimize the drawbacks associated with relevance-based filtering and model-based statistical optimization. A Random Forest criterion was used in the first step (Boruta) to filter and keep the most pertinent predictors out of the 18 initial predictors and only the statistically significant features were sent to the next round. These features were narrowed down by the second stage which involved the BSR with WASPAS evaluating several subsets in terms of statistical signals like Mallows Cp, Adjusted R^2, MSE, and AIC. The BSR created possible subsets, and the WASPAS approach combined all these various performance indicators into one composite ranking to create the most optimum and balanced subset. This two-step strategy enabled us to not only take advantage of Boruta that could identify all the variables of interest but also WASPAS-BSR, which was capable of trade-off between the statistical performance and the model parsimony, and as a result, strong and non-redundant selection of input variables.

2.3. Machine learning techniques

2.3.1. Deep neural network (DNN)

DNN is a modernized version of the artificial neural networks (Subasi, 2020). The DNN architecture comprises multi-layered nonlinear processing neurons to embody the abstraction of high-level data and execute a number of computer algorithms (Naskath et al., 2023). Based on the literature available, deep learning is superior in performance and scalability compared to outdated models of machine learning (Subasi, 2020). In addition, the learning process of DNN aims at producing precise output by continuously applying the feedforward and error back-propagation models (Ravindran et al., 2021). The activation function is significant in DNN to define the ability of the model to generalize. The number of available activation functions is large, although the most popular ones are the rectified linear unit (ReLU), hyperbolic tan, and the logistic sigmoid (Zhu et al., 2018). Their selection depends on the type of problem. The main equations of DNN are similar to the ANN model, with the difference that the DNN model has more layers and nodes. Suppose that x_i is the ith input to the node of a neural network, w_i is the weight of the ith input, b is the bias term, n is the number of inputs, and o is the output of the node. Then,

$$o = \sigma\left(\sum_{i=1}^{n} w_i x_i + b\right) \tag{11}$$

Where σ is the activation function.

Additionally, deep learning has several advantages, such as (i) automatic extraction of abstract features (representations) from the raw data, (ii) learning and storing the extracted features in the form of a trained network, and reusing the model trained on one task to another task through transfer learning, and (iii) increased network depth permits exponential development of the capability to characterize complex functions (Shen, 2018). Here, DNN is discussed briefly. For more information about the DNN, refer to Subasi (2020) and Shen (2018). Details of hyperparameter tuning are presented in Sections 2–5.

2.3.2. K-nearest neighbors (KNN)

In machine learning, the K-Nearest Neighbors (KNN) algorithm is an instance-based learning procedure (Altman, 1992). It operates under the concept of close proximity. The algorithm examines the 'K' closest labeled instances in the feature space, which are often referred to as the new instance's nearest neighbors when a new instance is introduced. The majority label of these neighbors is then used to classify the new instance. The algorithm is significantly influenced by the value of 'K'. A lower 'K' value can capture disturbance in the data, whereas a higher 'K' value can smooth over the data, potentially omitting smaller but significant patterns. The optimal 'K' value is typically contingent upon the specific dataset and problem at hand. The following equation can be used to determine the distance between two points 'p' and 'q' in an 'n-dimensional space using the Euclidian distance method:

$$d(p,q) = \sqrt{\sum_{i=1}^{n} (q_i - p_i)^2} \tag{12}$$

2.3.3. Support vector regression SVR

Support Vector Regression (SVR) is an elastic method of establishing the level of acceptable error in the model by using a hyperplane to fit the data (Vapnik et al., 1996). The SVR concept was firstly proposed by Drucker et al. that were based on the idea of support vectors by Vapnik. The main goal of SVR is to make the error rate to be always as minimal as possible. This is done through the introduction of a hyperplane and maximization of the gap between the predicted and actual values. Linear SVR can be characterized as the formula below:

$$y = \sum_{i=1}^{N} (a_i - a_i')\langle x_i, x\rangle + b \tag{13}$$

Here 'y' represents the predicted output, 'N' is the total count of observations, 'a_i' and 'a_i'' are the Lagrange multipliers for each observation, 'x_i' denotes the 'i-th' observation, 'x' is the input vector, 'b' is the bias term, and the angle brackets indicate the dot product between 'x_i' and 'x'.

2.3.4. KRR (Kernel ridge regression)

Kernel Ridge Regression is a nonparametric regression model that combines ridge regression with the kernel method (Rezaei et al., 2023). It can model linear and nonlinear relationships between predictor variables and outcomes. Kernel regression is relatively more complex than the usual least squares method and transforms smooth data into smaller steps. When dealing with high-dimensional data, the solution can be achieved using a kernel, making it easier to handle with less computing power. Another issue of Kernel Ridge Regression is overfitting data, which can be fixed by fine-tuning the model's parameters.

2.3.5. Elastic net

Zou and Hastie (2005) proposed the idea of the Elastic net. It is a multi-regression model that adds a penalty to combine the advantages of the Lasso and ridge regression (Zou and Hastie, 2005). On the other hand, the EN model uses the regularization technique to prevent overfitting and improve the prediction accuracy of the statistical model (Liu and Li, 2017). EN model also helps to select the significant input variables and find a simple model with the most appropriate independent variables (Al-Jawarneh et al., 2021). The EN regression model is written as (Al-Jawarneh et al., 2021; Narisetty, 2020):

$$\widehat{\beta}^{EN} = \underset{\beta}{\operatorname{argmin}} \left[\sum_{i=1}^{n} \left(y_i - \sum_{j=1}^{p} x_{ij}\beta_j \right)^2 + \lambda_1 \sum_{j=1}^{p} |\beta_j| + \lambda_2 \sum_{j=1}^{p} (\beta_j)^2 \right] \tag{14}$$

Where, y_i = output variable, $x_{ij} = j^{th}$ input variable of the i^{th} observation. Further, λ_1 and λ_2 = tunning parameters ($\lambda_1, \lambda_2 > 0$), and automatically selected during the cross-validation. These parameters control the regularization and nominate the input (predictor) variables (Zou and Hastie, 2005) and are represented as $\lambda_1 = 2n\lambda\alpha$, and $\lambda_2 = n\lambda(1-\alpha)$, then above equation becomes (Al-Jawarneh et al., 2021; Haws et al., 2015):

$$\widehat{\beta}^{EN} = \underset{\beta}{\operatorname{argmin}} \left[\frac{1}{2n} \sum_{i=1}^{n} \left(y_i - \sum_{j=1}^{p} x_{ij}\beta_j \right)^2 + \lambda \left(\alpha \sum_{j=1}^{p} |\beta_j| + \frac{1-\alpha}{2} \sum_{j=1}^{p} (\beta_j)^2 \right) \right] \tag{15}$$

Where α = regularization parameter ranges between 0 and 1. If $\alpha = 0$ represents the ridge regression, while $\alpha = 1$ signifies the Lasso regression. The two penalties, i.e., L_1 (Lasso) is used to obtain the sparsity and L_2 (ridge) is used to stabilize the L_1. Refer to Zou and Hastie (2005) for more background on elastic net readers.

2.4. Satin bowerbird optimizer (SBO)

Moosavi and Bardsiri (2017) initially discovered the concept of the SBO algorithms, enthused by the lifestyle of the Satin Bowerbird. Recently, the SBO has used applications in different domains, such as the estimation of software development effort (Moosavi and Bardsiri, 2017), congestion management in the deregulated power system (Chintam and Daniel, 2018), simulation of house energy management system (Chellamani and Chandramani, 2020), and prediction of electrical power (Moayedi and Mosavi, 2021). The working principles of the SBO algorithms include the following stages:

I. **Generate a set of random bowers:** During this stage, a set of random populations is generated with the position of the bowers. Each position is defined as an *n*-dimensional vector of the parameters that must be optimized (Chintam and Daniel, 2018). The integration of the parameters determines the effectiveness of the bowers.

II. **Calculate the probability of each population member:** Using Eq. (16), the probability of attractiveness of a bower is calculated as (Liu and Liang, 2024):

$$Prob_i = \frac{Fit_i}{\sum_{n=1}^{NB} Fit_n} \tag{16}$$

$$Prob_i = \begin{cases} \dfrac{1}{1+f(x_i)} & f(x_i) \geq 0 \\ 1 + |f(x_i)| & f(x_i) < 0 \end{cases} \tag{17}$$

where Fit_i defines the fitness of the i^{th} the solution, NB denotes the number of bowers, and $f(x_i)$ describes the cost function value in i^{th} position or bower.

III. **Elitism:** It is a crucial characteristic of evolutionary algorithms that enables the retention of optimal solutions at each phase of the optimization process. Eq. (17) is based on the comparison of the cost function values in the elitism step to select the best-fitted member. Hence, the bowerbird with the highest fitness has a better solution (Chintam and Daniel, 2018; Liu and Liang, 2024).

IV. **Estimate the new variations in any positions:** By using Eq. (18) in each cycle of the model, the new variations at any bower are estimated as (Moosavi and Bardsiri, 2017):

$$X_{ik}^{new} = X_{ik}^{old} + \lambda_k \left(\left(\frac{x_{jk} + x_{elite,k}}{2} \right) - X_{ik}^{old} \right) \tag{18}$$

In Eq. (19), X_i describes the i^{th} solution vector, X_{ik} indicates the k^{th} member of this vector, x_j defines the target solution between all solutions in the current iteration. The j is obtained using the roulette wheel procedure, and x_{elite} states the position of the elite (saved in each cycle of the algorithm). The attraction power of the goal bower is projected by λ_k parameter, also known as the step length factor for the k^{th} element in the position of the vector.

2.4.1. Mutation

During mutation, in a dating competition, the weaker bowers are destroyed by the strong and experienced bowerbirds. Resulting in a mutation process and demarcated as (Chen et al., 2021):

$$X_{ik}^{new} \sim N(X_{ik}^{old}, \sigma^2) \tag{19}$$

$$\sigma = z \times (\text{var}_{\max} - \text{var}_{\min}) \tag{20}$$

here, $\text{var}_{\max}$ and $\text{var}_{\min}$ express the maximum and minimum values allocated to the variables, z outlines the adjustment factor, and σ labels the proportion of space width.

2.4.2. Merge the old and new populations obtained from variations

At this step, the old population and the population derived from variations are evaluated at the conclusion of each cycle (Moosavi and Bardsiri, 2017). After that, these two populations are merged and preserved, a new population is created, and others are removed. The process is terminated when the best solution is obtained. If not, continue the stages II through V for the next cycle (Chintam and Daniel, 2018; Liu and Liang, 2024).

2.5. Deep neural network combined with satin bowerbird optimizer (DNN-SBO)

Superior performance of a Deep Neural Network (DNN) on complex tasks requires tuning of its hyperparameters. Learning rate, batch size, number of layers, number of neurons per layer, and number of epochs are key hyperparameters. The learning rate determines how much to correct the weights towards the loss gradient, influencing convergence speed by being too high, resulting in overshooting minima, or too low, resulting in slow training speed. For instance, the batch size (i.e., the number of samples processed per step) controls the size of the model's internal parameters that are updated; with smaller batches we are given a noisy but wide-ranging view; with bigger batches we are given a more robust but narrower view. The depth of the network is defined by the number of layers and captures higher-level abstractions since there may be too few or too many, and hence it may lead to overfitting. The model's expressive power depends on the number of neurons in each layer, resulting in the need to find a balance to avoid overcomplexity. The epochs refer to how many times the training process goes through the whole dataset; possibly too few epochs may result in underfitting, as not enough training is given. Thus, Mean Squared Error (MSE) is used as the fitness function to optimize the model by checking the prediction errors systematically. To aid this process, the Satin Bowerbird Optimizer (SBO) was designed to simulate the mate selection behaviors of satin bowerbirds to lead an exploration and exploitation based creative search for optimal hyperparameter values in an iterative manner. SBO's mechanism, which is introduced using moderate changes to the hyperparameters, works to "fine-tune" a DNN on better performance metrics for accuracy and stability on different datasets. The schematic structure of the DNN-SBO model is shown in Fig. 2.

2.6. SHAP explainable AI

In recent times, the SHAP technique has been utilized immensely to enhance the prediction obtained from machine learning models. The idea of the SHAP was given by Shapley (1953) based on the game theory concept. The SHAP method explains predictions by computing the contributions of distinct parameters in terms of Shapley values and highlights the most significant factors and their connections in defining the desired output (Kellner et al., 2022; Utama et al., 2023). Eq. (21) defines the mathematical form of the SHAP (Dikshit and Pradhan, 2021; El Bilali et al., 2023):

$$\phi_i(ML, x) = \sum_{t \subseteq x\{i\}} \frac{|t|!(n - |t| - 1)!}{n!} [ML(t) - ML(t \backslash i)] \tag{21}$$

Here, n defines the number of input features, $\phi_i \epsilon R$ describes the contribution of variable i to the ML model, and explains the difference-set notation for set operations. Then, the explanation model is employed to clarify the outcome of each observation by precisely calculating the SHAP value of each feature for that observation, which is expressed as

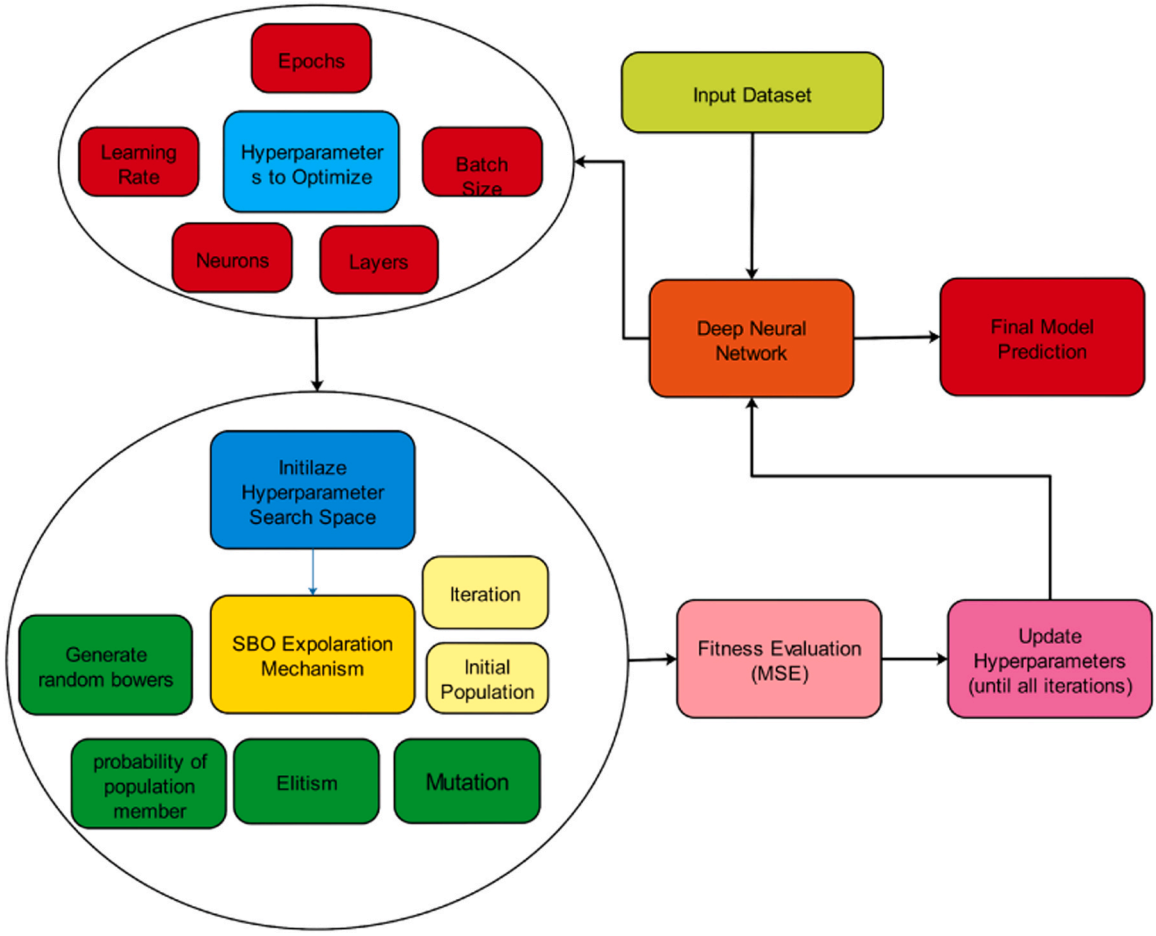

Fig. 2. – Schematic structure of DNN-SBO model.

(Dikshit and Pradhan, 2021; El Bilali et al., 2023):

$$EM = \phi_0 + \sum_{i=1}^{M} \phi_i t_i \tag{22}$$

where $t_i \epsilon \{0,1\}^M$ and M define the simplification of the input feature, ϕ_0 indicates the base value of the prediction model and ϕ_i is the Shapley value for feature i. For more details about the SHAP and different AI model explainers, readers refer to Shapley (1953) and Molnar (2020).

2.7. Performance metric

Assessing the performance of the provided intelligent frameworks is crucial for the prediction of yield values. In this study, we employed six diverse statistical indices to evaluate the accuracy of these techniques: Correlation Coefficient (R), Root Mean Square Error (RMSE), Uncertainty coefficient of 95% confidence (U95 %), Mean Absolute Percentage Error (MAPE), and Kling–Gupta Efficiency (KGE) (Gupta et al., 2009; Jangid et al., 2025). The mathematical formulas of these performance metrics are as follows:

$$R = \frac{\sum_{i=1}^{N} \left(Y_{o,i} - \overline{Y_o}\right)\left(Y_{p,i} - \overline{Y_p}\right)}{\sqrt{\sum_{i=1}^{N} \left(Y_{o,i} - \overline{Y_o}\right)^2 \sum_{i=1}^{N} \left(Y_{p,i} - \overline{Y_p}\right)^2}} \tag{23}$$

$$RMSE = \sqrt{\frac{1}{N} \sum_{i=1}^{N} \left(Y_{o,i} - Y_{p,i}\right)^2} \tag{24}$$

$$U_{95\%} = 1.96\sqrt{SD_e^2 + RMSE^2} \tag{25}$$

$$NS = 1 - \frac{\sum_{i=1}^{N} \left(Y_{p,i} - Y_{o,i}\right)^2}{\sum_{i=1}^{N} \left(Y_{o,i} - \overline{Y_o}\right)^2} \tag{26}$$

$$MAPE = \frac{1}{N} \sum_{i=1}^{N} \left| \frac{Y_{o,i} - Y_{p,i}}{Y_{o,i}} \right| \times 100 \tag{27}$$

$$KGE = 1 - \sqrt{(R-1)^2 + (\alpha - 1)^2 + (\beta - 1)^2} \tag{28}$$

$$\alpha = \frac{Y_{p,i}}{Y_{Po,i}} \beta = \frac{CV_p}{CV_s}$$

where $Y_{o,i}$ is measured yield value, $Y_{p,i}$ is the predicted yield value, and N denotes the total number of datasets in each phase of the modeling. Besides, the α and β represent the relative standard deviation of the predicted and measured yield values and the ratio of the average predicted yield value to the average measured yield value. SD_e is the standard deviation of errors computed using ($Y_{o,i} - Y_{p,i}$). The Correlation Coefficient (R) assesses linear relationships between measured and predicted values, ranging from −1 (perfect negative) to 1 (perfect positive). A value of zero indicates no linear relationship, while higher positive values signify a strong positive correlation. Kling-Gupta Efficiency (KGE), a metric incorporating correlation, variability, and bias, measures model performance within a range of -∞ to 1. A KGE of 1 signifies perfect alignment between measured and predicted values, zero indicates performance equivalent to the mean of observed values, and

values below zero suggest poorer performance than using the mean of observed values. Uncertainty Coefficient ($U_{95\,\%}$) determines the confidence interval surrounding predictions, representing the range where actual values likely fall with 95 % confidence. Ranging from zero to ∞ . Lower $U_{95\,\%}$ values indicate less uncertainty and more reliable accuracy, while higher values suggest greater uncertainty and less promising accuracy. Overall, higher values of R, KGE, and NS alongside lower values of RMSE, MAPE, and $U_{95\,\%}$ signify the superior performance of the understudy model.

2.8. Research methodology

This section outlines the process for assessing potato tuber yields in Maritime Canadian provinces (New Brunswick and Prince Edward Island) using a new Interpretable expert system comprised of the Deep Neural Network integrated with Satin-Bowerbird (DNN-SBO) Optimization algorithm supported by Boruta-BSR-WASPAS feature filtering strategy and SHAP explainer. This study incorporates soil characteristics data points (New Brunswick|241 and PEI|315), encompassing 18 field features such as Organic Matter, pH, Phosphate (P_2O_5), Potash (K_2O), Calcium (Ca), Magnesium (Mg), Brom (B), Copper (Cu), Zinc (Zn), Sulfur (S), Manganese (Mn), Iron (Fe), Sodium (Na), Aluminum (Al), Lime Index, % P/Al, CEC, and Total Base Saturation.

Here, four classical comparative models, including the Elastic Net, KRR, SVR, and KNN, were incorporated with the first stage of preprocessing (Boruta-BSR-WASPAS) to validate the predictive performance of the main model aimed at the yield potato estimation. Elastic Net, KRR, SVR, and KNN machine learning models are implemented using the open-source Scikit-learn library on the Python platform, whereas the DNN was performed using the Tensorflow library. Moreover, the SBO algorithm (Moosavi and Bardsiri, 2017), Boruta feature selection, BSR scheme, and SHAP explainer tool have been provided through the Mealpy, Boruta, Scikit-learn (Pedregosa et al., 2011), and SHAP libraries. Notably, all computations are performed on a personal laptop with 32.0 GB RAM and an Intel Core i7 processor running at 2.60–3.40 GHz. Fig. 3 illustrates the modeling phases for predicting potato yield using this advanced optimized deep learning algorithm, namely the Boruta-BSR-WASPAS integrated with the DNN-SBO model.

3. Results

In this section, the results of the research are made in a systematic way. First, Section 3–1 presents the outcome of the operations of feature selection, and the most important soil properties which were identified by the multi-stage approach in the selection. Section 3–2 presents the predictive accuracy of proposed DNN-SBO model and comparative machine learning models (Elastic Net, KRR, SVR, and KNN) with various combinations of inputs features. Further model evaluation and explainability analysis using SHAP values described in subsequent subsections (3−3−3−5) is necessary. All these findings testify to the

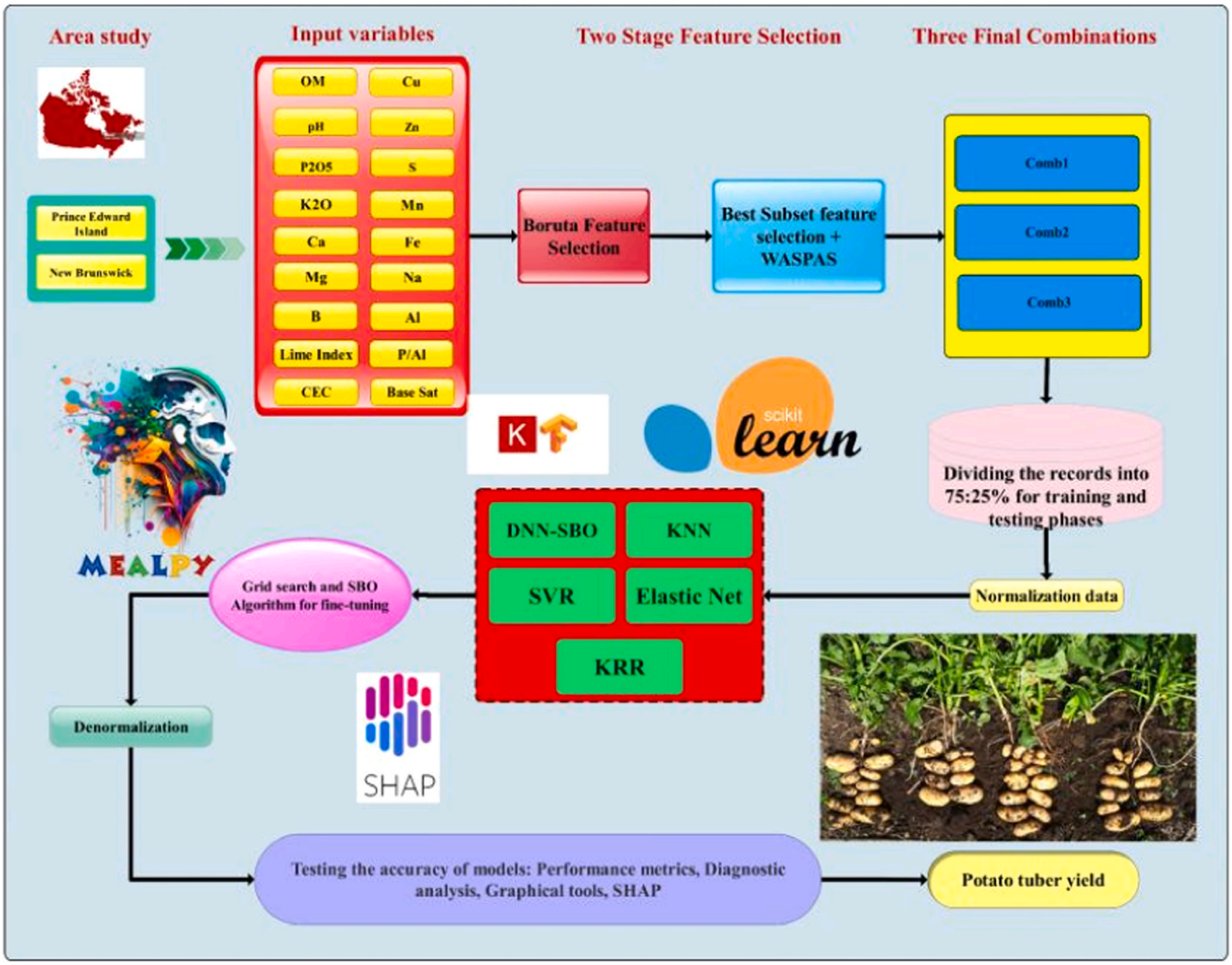

Fig. 3. Research flowchart.

validity and applicability of the suggested framework to predict potato yield.

3.1. Feature selection results

The small predictability of current datasets in agriculture regarding the yield of potatoes means that it is important to identify the most effective predictors of potato yield using an effective pre-processing phase where nonlinear relationships between predictors and outcomes are taken into account. To do this, the Boruta feature selection method has been applied in order to stress the significant predictors according to Z-score, and the Max-Shadow criterion has been applied to drop off the redundant features to achieve the best predictive performance. Fig. 4 box-plot graphs show the 12 significant features detected that are represented by green color. The parameters that have the greatest influence include Total Base Saturation, Sulfur, Magnesium, Potash, Calcium, Aluminum, Zinc, Manganese, Organic Matter, Iron, and Copper. These parameters will be the input in the form of candidate combinations that will feed the models. It is important to note that tentative features are represented by the yellow color, whereas rejected features are represented by the red color in the box-plot. The next step of preprocessing consisted of the selection of optimal input combinations which was based on a new approach named BSR-WASPAS that applied Mallows Cp, AIC, and Pc measurements. To begin with, the best subset Regression (BSR) method was used to identify the top ten possible combinations. Then, all the indices were personalized with the help of Weighted Aggregated Sum Product Assessment (WASPAS) with weights that had the same significance. The minimum values of C_p, AIC and P_c as well as maximum values of Adjusted R-squared (Adj-R^2) were taken into account with the purpose to calculate WASPAS values of each combination of candidates. Finally, three combinations that are associated with the lowest values of WASPAS were interpreted to be the most favorable input combinations to feed the given model. The combinations were Combo 1 (WASPAS=0.194), Combo 2 (WASPAS=0.208) and Combo 3 (WASPAS=0.26). The results of this second preprocessing are summarized in Table S2 (Success Supplemental Material) according to these criteria. The 556 data points were randomly chosen as the training and testing sets. Specifically, 75 % of the data was to be used in the training, and the remainder or 25 % was to be used in the testing.

The training subset was performed through a k-fold cross-validation with ten folds to avoid overfitting the model's outcomes. The testing and training sets were normalized to a range of [0, 1] before applying the machine learning techniques to enhance convergence and ensure model stability.

Tuning hyperparameters is crucial for soft computing models as they significantly impact their accuracy. In this study, the DNN-SBO model contains four critical hyperparameters: hidden_layer_sizes, learning_rate, batch_size, and epoch value, which have been accurately estimated using the Surrogate-Based Optimization (SBO) algorithm through the Mealpy library. A grid search strategy was also employed to tune

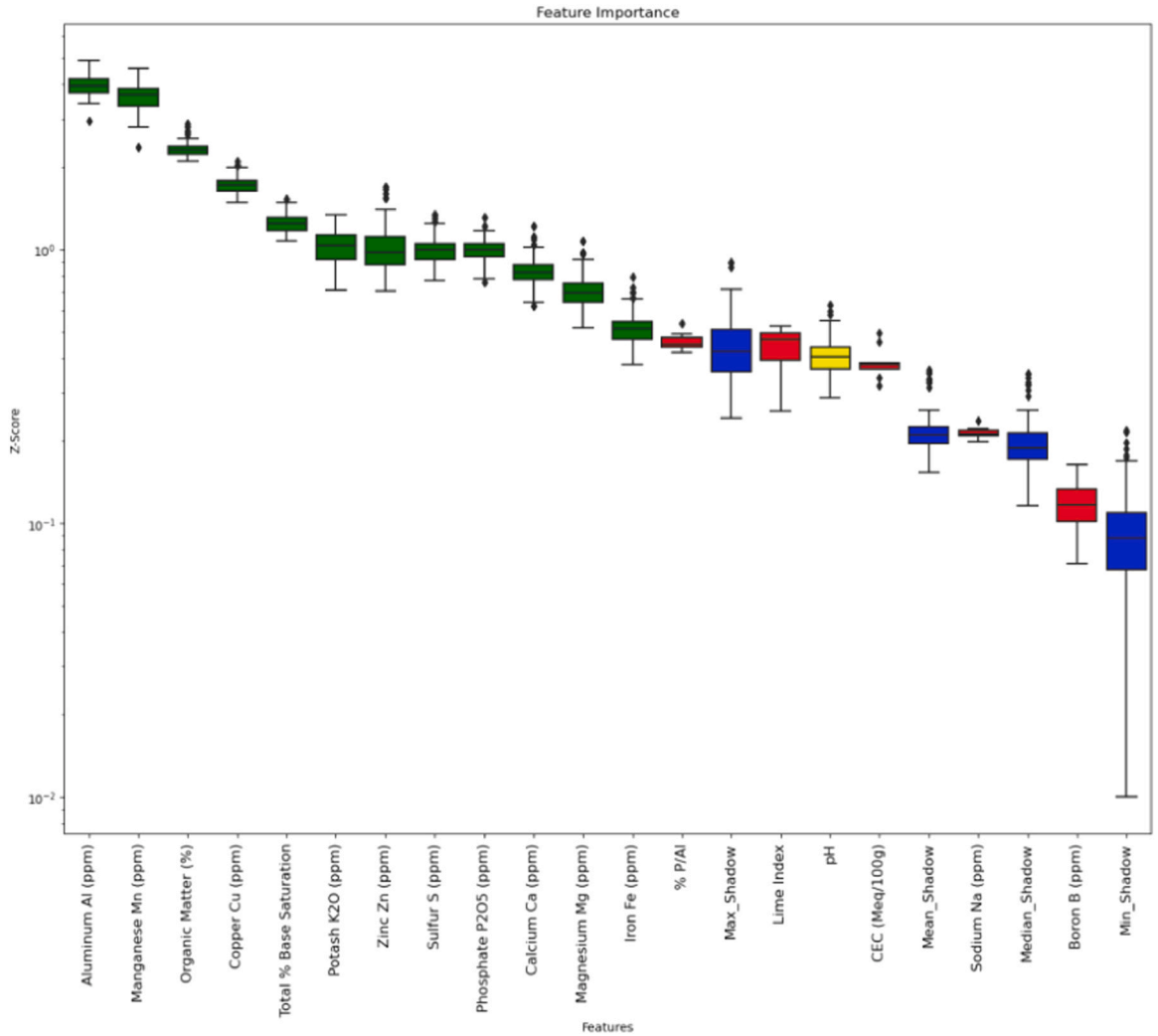

Fig. 4. Boruta feature selection results.

comparative ML models: Elastic Net, KRR, SVR, and KNN. Table S3 summarizes the optimal hyperparameters for each model using SBO for DNN-SBO and the grid search strategy for the remaining ML models. The essential parameters of the comparative models are as follows: Elastic Net (Alpha, l1_ratio), KRR (alpha, gamma), SVR (C, Epsilon, Gamma), and KNN (n_neighbors). The SBO algorithm in this work was set to a population size of 10 individuals, maximum iteration count of 30, and a convergence threshold of the smallest variation of less than 10^{-5} of the objective function value within a ten consecutive iterations. These hyperparameters have been chosen according to initial sensitivity analysis in order to balance between the efficiency and stability of optimization.

3.2. Machine learning model results

The DNN-SBO, Elastic Net, KRR, SVR, and KNN models were evaluated both in training and testing periods based on Comb1, Comb2, and Comb3 using a set of standard statistical metrics, R, RMSE (t/ha), MAPE (t/ha), NS, KGE, and $U_{95\,\%}$ for potato yield prediction. Moreover, various types of diagnostic plots were also utilized to inspect the performance of the models.

Fig. 5 describes the assessment metrics in Radar plots using the input combinations Comb1, Comb2, and Comb3 based on the performance generated by DNN-SBO, Elastic Net, KRR, SVR, and KNN models to predict potato yield. It is apparent that the DNN-SBO model exhibits higher precision accuracy in terms of higher values of R, NS, KGE, $U_{95\,\%}$, and lower values of RMSE (t/ha), MAPE (%) against Elastic Net, KRR, SVR, and KNN models for Comb2 in relation to Comb1 and Comb3. Therefore, the DNN-SBO model performs better in predicting potato yield using Comb2.

Table 1 portrays the potato yield prediction performance of the models based on Goodness-of-fit metrics in the scenarios Comb1, Comb2, and Comb3. It is recorded that the DNN-SBO model accomplished better accuracy when using Comb2 by generating (R = 0.903, RMSE = 4.165, MAPE = 6.766, NSE = 0.807, KGE = 0.889, $U_{95\,\%}$ = 3.096) and (R = 0.853, RMSE = 5.522, MAPE = 9.707, NSE = 0.716, KGE = 0.843, $U_{95\,\%}$ = 4.126) in training and testing periods to predict potato yield as compared to Elastic Net, KRR, SVR, and KNN models. Moreover, the DNN-SBO model performs reasonably well using Comb 1 and Comb3 compared to the other models (see Table 1). However, the highest precision was registered by the DNN-SBO model with Comb2 to predict potato yield compared to the Elastic Net, KRR, SVR, and KNN models.

The scatter plots in Fig. 6 evaluate the usefulness of the DNN-SBO *vs.* Elastic Net, KRR, SVR, and KNN models between the observed and predicted potato yield using all three input combinations, Comb1, Comb2, and Comb3. The scatter plots explain the models' prediction skills by comparing these models, which newly incorporate R and RMSE metrics. It is clear from the Fig. 6 that for Comb2, the DNN-SBO model reached best performance in terms of R = 0.853, RMSE = 5.522, followed by KNN (R= 0.776, RMSE = 6.654), SVR(R = 0.770, RMSE = 6.621), KRR (R = 0.679, RMSE = 7.679), and Elastic Net (R = 0.549, RMSE = 8.761) to predict potato yield. Similarly, the DNN-SBO model outperformed Comb1 and Comb2 in achieving the highest accuracy compared to other models in predicting potato yield.

Fig. 7 presents a more detailed evaluation based on Swarm plots of the distribution of observed versus predicted potato yields along with IQR values using input combination Comb1 (C1), Comb2 (C2), and Comb3 (C3) for the DNN-SBO *vs.* Elastic Net, KRR, SVR, and KNN models. In addition, the Mean values were also inserted to measure the robustness of these newly proposed hybrid models. It is noticeable that the DNN-SBO model displayed more consistent Swarm plots with IQR = 11.21-C1, 11.68-C2, 7.731-C3 as compared to Elastic Net, KRR, SVR, and KNN models. Moreover, the IQR values of the DNN-SBO model were also close to the observed potato yield when using C2, followed by C1 and C3, as compared to other models. Hence, the DNN-SBO model accomplishes the best and most consistent accuracy in forecasting potato yield.

Fig. 8 offers a more detailed appraisal of the DNN-SBO *vs.* Elastic Net, KRR, SVR, and KNN models using input combination Comb1 (C1), Comb2 (C2), and Comb3 (C3) based on box-plots of relative errors to predict potato yield. In addition, the IQR values were also incorporated to measure the robustness of these models. The DNN-SBO model based on C2 displayed more consistent box-plots with a lower IQR = 15.88 compared to all other models. Moreover, the DNN-SBO model was reasonably good on C1 and C2 input combinations but performed best on C2. Hence, C2 appeared to be the most suitable input combination for the DNN-SBO model to predict potato yield.

3.3. Taylor diagrams

The Taylor diagrams in Fig. 9 detail the DNN-SBO, Elastic Net, KRR, SVR, and KNN models in Comb1, Comb2, and Comb3 to more deeply assess the models' efficiency between the observed and predicted potato yield. Taylor diagrams depict a thorough judgment to examine the model comparison centered on standard deviation and correlation coefficient for each input combination scenario. The DNN-SBO model is clearly positioned closer to the referenced precipitation with a correlation coefficient between 0.85 and 0.90 to predict the potato yield at Comb2, followed by Comb3 and Comb1. The SVR, KNN, and KRR models are also reasonably okay based on Comb2, positioned closely with 0.80 compared to Elastic Net, but could not surpass the DNN-SBO model. This proves that the DNN-SBO model predicted the potato yield with higher accuracy.

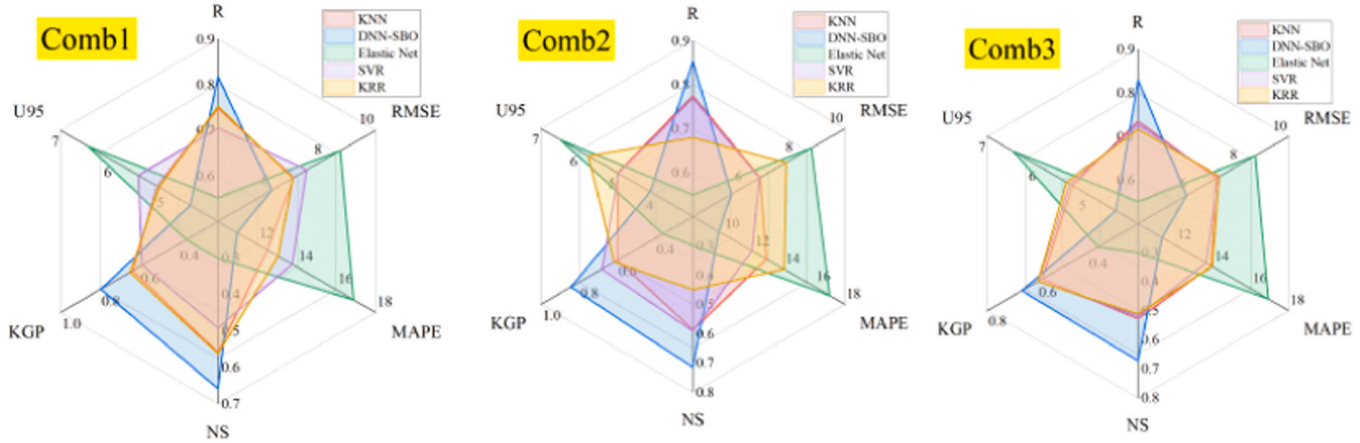

Fig. 5. Radar plots of performance metrics for different combinations.

Table 1
Results of machine learning techniques in yield prediction.

Scenario	Model	Data	R	RMSE (t/ha)	MAPE (%)	NS	KGE	$U_{95\,\%}$
Comb1	KNN	Train	0.878	4.593	7.969	0.766	0.771	3.439
		Test	0.748	6.884	12.505	0.558	0.633	5.160
	DNN-SBO	Train	0.850	5.004	8.156	0.722	0.796	3.747
		Test	0.818	6.046	10.973	0.659	0.796	4.531
	Elastic Net	Train	0.612	7.508	12.732	0.374	0.465	5.623
		Test	0.552	8.653	16.896	0.302	0.360	6.483
	SVR	Train	0.787	5.875	8.888	0.617	0.670	4.399
		Test	0.706	7.383	13.768	0.492	0.584	5.519
	KRR	Train	0.829	5.344	8.972	0.683	0.711	4.003
		Test	0.753	6.847	13.060	0.563	0.646	5.123
Comb2	KNN	Train	0.850	5.204	9.080	0.699	0.662	3.896
		Test	0.776	6.654	12.841	0.587	0.598	4.983
	DNN-SBO	Train	0.903	4.165	6.766	0.807	0.889	3.096
		Test	**0.853**	**5.522**	**9.707**	**0.716**	**0.843**	**4.126**
	Elastic Net	Train	0.615	7.487	12.746	0.378	0.470	5.607
		Test	0.549	8.671	17.001	0.299	0.358	6.496
	SVR	Train	0.908	4.012	5.109	0.821	0.830	3.004
		Test	0.770	6.621	11.900	0.591	0.680	4.962
	KRR	Train	0.788	5.847	9.906	0.620	0.696	4.379
		Test	0.679	7.679	14.007	0.450	0.614	5.758
Comb3	KNN	Train	0.881	4.613	8.194	0.764	0.741	3.453
		Test	0.735	7.113	13.896	0.528	0.582	5.308
	DNN-SBO	Train	0.828	5.427	9.169	0.673	0.716	4.034
		Test	0.830	5.927	11.280	0.672	0.662	4.441
	Elastic Net	Train	0.612	7.509	12.726	0.374	0.465	5.623
		Test	0.551	8.663	16.915	0.300	0.360	6.490
	SVR	Train	0.884	4.497	6.100	0.775	0.779	3.368
		Test	0.728	7.182	13.612	0.519	0.596	5.359
	KRR	Train	0.812	5.568	9.445	0.656	0.690	4.170
		Test	0.717	7.242	13.937	0.511	0.599	5.424

3.4. Uncertainty analysis

Any predictive model's reliability must be evaluated in order to estimate and predict output with accuracy and consistency. Uncertainty analysis (UA) is used throughout this study to evaluate the quantitative assessment of the error of the models utilized for predicting the yield values. These parameters include the absolute error (AE), standard deviation (SD), standard error (SE), margin of error (ME), lower bound (LB), upper bound (UB), and width of confidence bound (WCB). The difference between the upper and lower bounds is known as the width of the confidence bound (WCB). The results of the uncertainty analysis are depicted in Table 2. According to this table, it can be seen that in each input combination, the DNN-SBO model has the least width of confidence bound (WCB) and other reported metrics. A comparison among different input scenarios shows that combination 2 has lower metric values. So, the uncertainty analysis result is in accordance with previous findings. Fig. 10. Shows the uncertainty interval plots for our superior model (DNN-SBO) in three different scenarios.

3.5. Explainability analysis

The explainability and interpretability graphs in Fig. 11 show the SHAP analysis for the global interpretation of each input predictor using the DNN-SBO model. The SHAP analysis judges the influence of the input predictors on the DNN-SBO models' prediction of potato yield. The mean SHAP value (Fig. 11.A) and correlation coefficient (Fig. 11.B) identify that the input predictor Iron has the highest contribution to the model's output prediction with the highest mean SHAP value = +5.49, which is also supported by the correlation coefficient value = 0.298 and appeared to be the most positively impacted factor. The input predictors, organic Matter, total base saturation, manganese, Aluminum, and magnesium, positively impact the model's potato yield prediction, confirmed by the mean SHAP values and coefficient correlation. Thus, it is clear that Iron is the strongest and the main contributing predictor to the model's potato yield prediction.

The ribbon plot in Fig. 12 indicates the efficiency of each input predictor based on SHAP analysis for different ranges of potato yield. It is clear that Iron was the most significant factor in all three ranges, and it is a contributor to the DNN-SBO model output. For example, in the low range, the SHAP value is 4.86 for the iron input predictor, whereas it is 5.24 and 6.37 for the medium and high ranges of potato yield. Copper performs better in low and high ranges, whereas zinc is good in medium ranges. More details of the SHAP analysis for different ranges of potato yield for other input predictors can be seen in Fig. 12.

4. Discussion

The current study introduces a new ML framework, DNN-SBO, that integrates the Satin Bowerbird Optimizer with a Deep Neural Network to predict potato yields in the Canadian Maritime provinces.

4.1. Input data

This framework is unique primarily because it concentrates on a broad range of soil properties, such as iron, copper, organic matter, cation exchange capacity, and others, to assess yield in Prince Edward Island and New Brunswick. The emphasis on soil-level data is unlike many existing potato-yield studies that often incorporate remote-sensing indices (e.g., UAV or satellite imagery), meteorological variables (temperature, rainfall), or management practices (irrigation or pest control) (Fan et al., 2024). For instance, Tamayo-Vera et al. (2024), (2025) effectively used climate data and remote sensing features combined with tree-based models like Random Forests to predict regional potato yields in Prince Edward Island, capturing temporal dependencies and environmental variability (Tamayo-Vera et al., 2025) (Tamayo-Vera et al., 2024). By directing feature selection via Boruta, Best Subset Regression, and the WASPAS method, this research ensures that only those soil variables with demonstrated predictive value are ultimately used by the DNN-SBO algorithm.

A notable feature of the present approach lies in its exclusive focus on soil attributes. Several earlier efforts—such as (Abrougui et al., 2019) (Mishra et al., 2023) (Kurek et al., 2023) —have tested more diverse

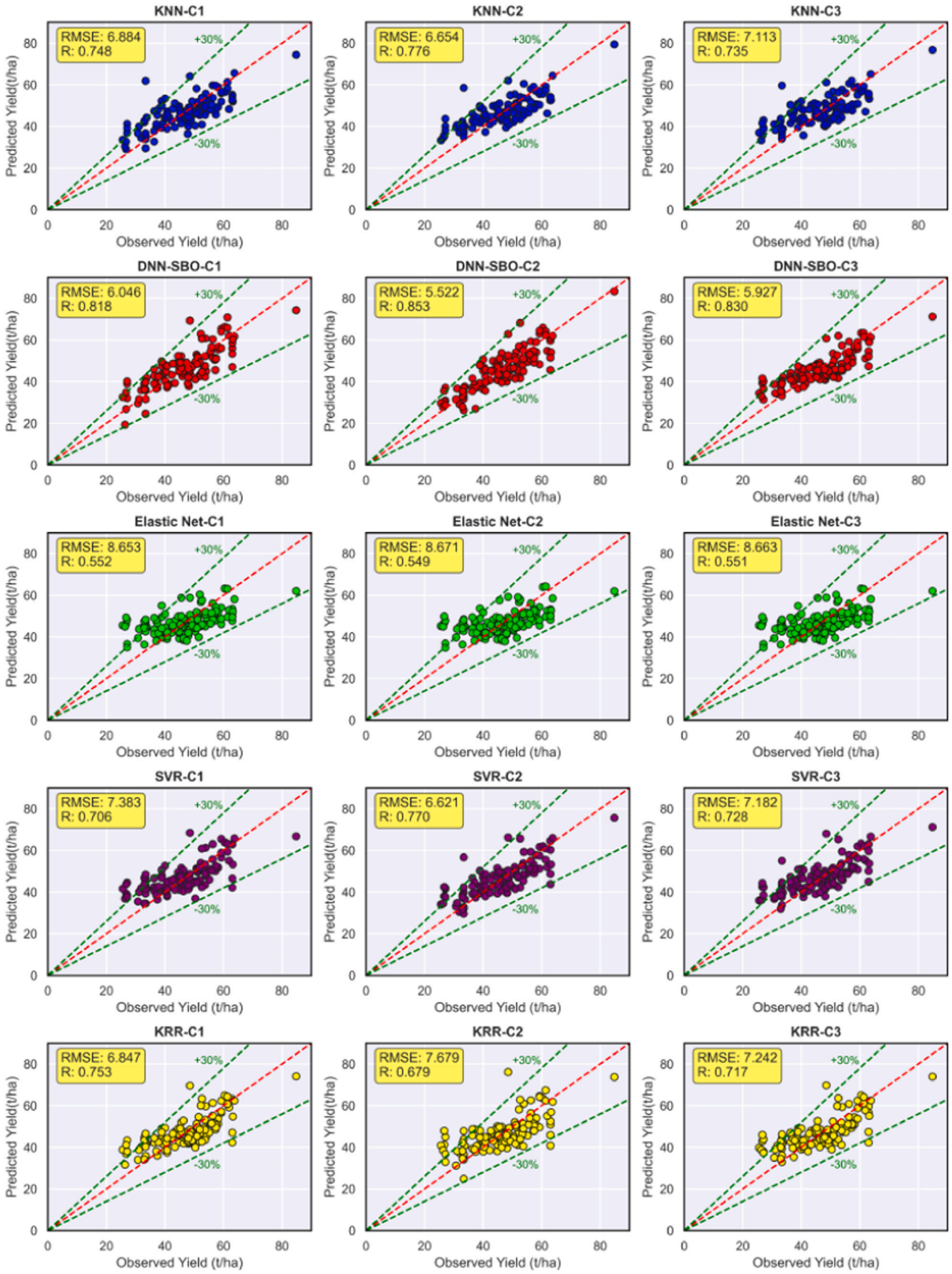

Fig. 6. Scatter plots of observed versus predicted values for all models and combinations.

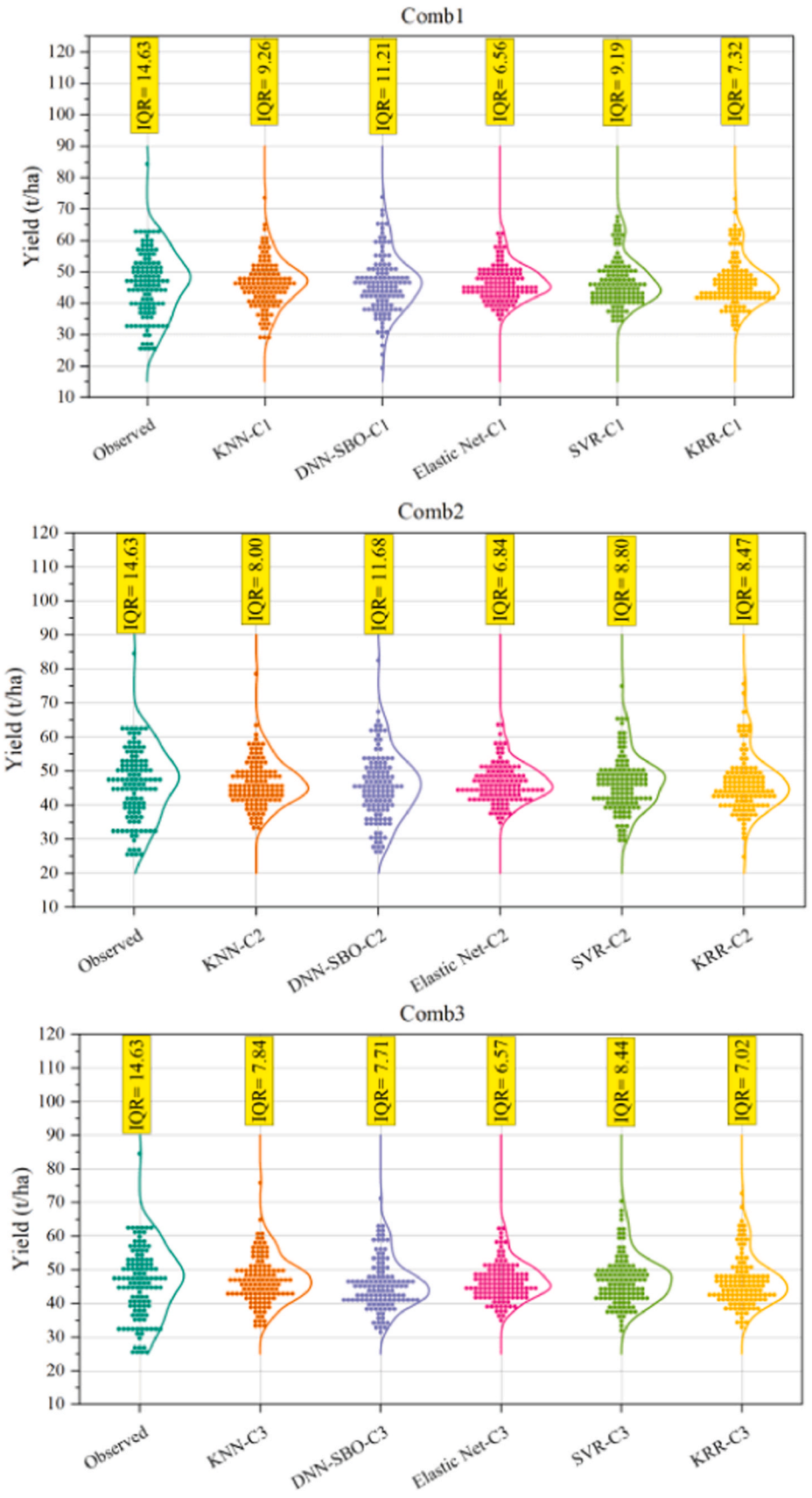

Fig. 7. Swarm plots of the distribution of observed values of yield versus predicted values for different input combinations.

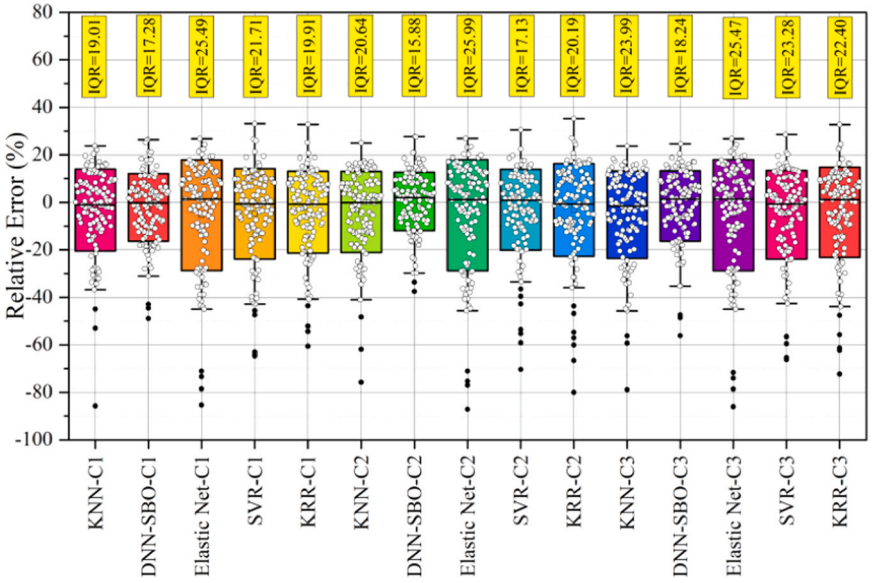

Fig. 8. Box-plots of relative error.

data sources, combining agronomic variables like fertilizer applications or pest incidence with weather-based indicators. Others incorporated advanced techniques, for instance, merging remote-sensing reflectance data and field measurements (Subramaniam and Marimuthu, 2024) or applying cutting-edge ensemble models with climate and topographical inputs (El-Kenawy et al., 2024), (Eed et al., 2024). While these broader methods can capture environmental and management effects, the soil-centered design of this study underscores the strong direct link between nutrient availability and final tuber yields. The comparatively few studies (e.g., (Abrougui et al., 2019)) that focus heavily on soil chemical and physical properties have so far employed simpler machine-learning or regression methods, making DNN-SBO's results especially noteworthy. With a maximum testing R-value of 0.853 using the top input combination (Comb2), the proposed pipeline demonstrates that meticulously chosen soil variables can, in some contexts, yield accurate crop predictions.

4.2. Machine learning models

Various machine learning and deep learning algorithms have been widely employed across yield prediction studies, including Support Vector Regression (SVR), Kernel Ridge Regression (KRR), K-Nearest Neighbors (KNN), Random Forests (RF), Convolutional Neural Networks (CNN), Long Short-Term Memory (LSTM) networks, Graph Neural Networks (GNN), and hybrid ensemble models ((El-Kenawy et al., 2024), (Piekutowska and Niedbała, 2025), (Kuradusenge et al., 2023), (Li et al., 2021)). These models are typically trained on heterogeneous datasets containing both environmental and management variables, and tuned using common methods such as grid search or randomized searches to optimize their hyperparameters.

The DNN-SBO model proposed here stands out due to the integration of the Satin Bowerbird Optimization metaheuristic to fine-tune critical hyperparameters of the deep neural network. This approach resulted in superior predictive accuracy, outperforming traditional models like Elastic Net, SVR, KNN, and KRR in all tested scenarios, especially with the optimal soil feature combination (Comb2). The metaheuristic optimization enables efficient exploration of the hyperparameter space, mitigating common issues such as local minima and overfitting that more conventional tuning methods may face ((Seyyedabbasi et al., 2021), (Jia et al., 2024)).

The high accuracy of the DNNSBO model may be explained by the combination of the deep network architecture and evolutionary optimization strategy. The multilayered DNN is an effective way of modeling the nonlinear and the high-order interactions of soil properties and yield so that the model can be used to approximate the complex functional relationships, which are not possible with linear or ensemble models. Moreover, the SBO algorithm is an improvement of the tuning process, which uses a population-based search that adjusted hyperparameters with a balance of exploration as well as exploitation. In contrast to traditional methods of optimization that can become stuck in local minima, SBO keeps a large, varied set of candidate solutions and evolves them during each iteration (based on the learning performance) and so through the training process the evolution can approach globally optimal configurations. This combination has more generalization capacity, less overfitting and more frequent predictive stability across validation runs than gradient-based or heuristic tuning alone.

A critical examination of the DNN-SBO model's superior accuracy compared to conventional approaches (Elastic Net, SVR, KNN, and KRR) is equally important. The use of a specialized metaheuristic (SBO) to calibrate the deep neural network's hyperparameters has allowed the model to capture potentially non-linear relationships. Moreover, the multi-stage feature-selection pipeline of Boruta-BSR-WASPAS represents a more systematic approach to isolating key soil parameters, thereby improving the overall model stability. Studies that rely on single-step or default feature filtering can find their predictions hampered by noisy or irrelevant variables. This advanced methodology, which merges the cutting-edge DNN and optimization, paves the way for a more precise data-driven yield model.

4.3. Results interpretability

The paper also uses model explainability with Shapley Additive Explanations (SHAP) to make the contribution of individual variables in the soil to the model yield explanations. The ranking of iron as the most common predictive characteristic, copper, zinc, phosphorus, and organic matter are all as expected in agronomics and can be used to act on the insights of the stakeholders. This explainability aspect tackles a typical deep-learning problem, namely the black box models, which is the aspect that is less prevalent in prior yield prediction studies. Iron (Fe) is an important micronutrient that is required in the synthesis of chlorophyll, in electron transport during photosynthesis, and in enzymes used in nitrogen metabolism (Marschner, 2011). The sufficient Fe provision improves photosynthetic efficiency and biomass gain, and deficiency causes chlorosis, hindered root activity, and a significant

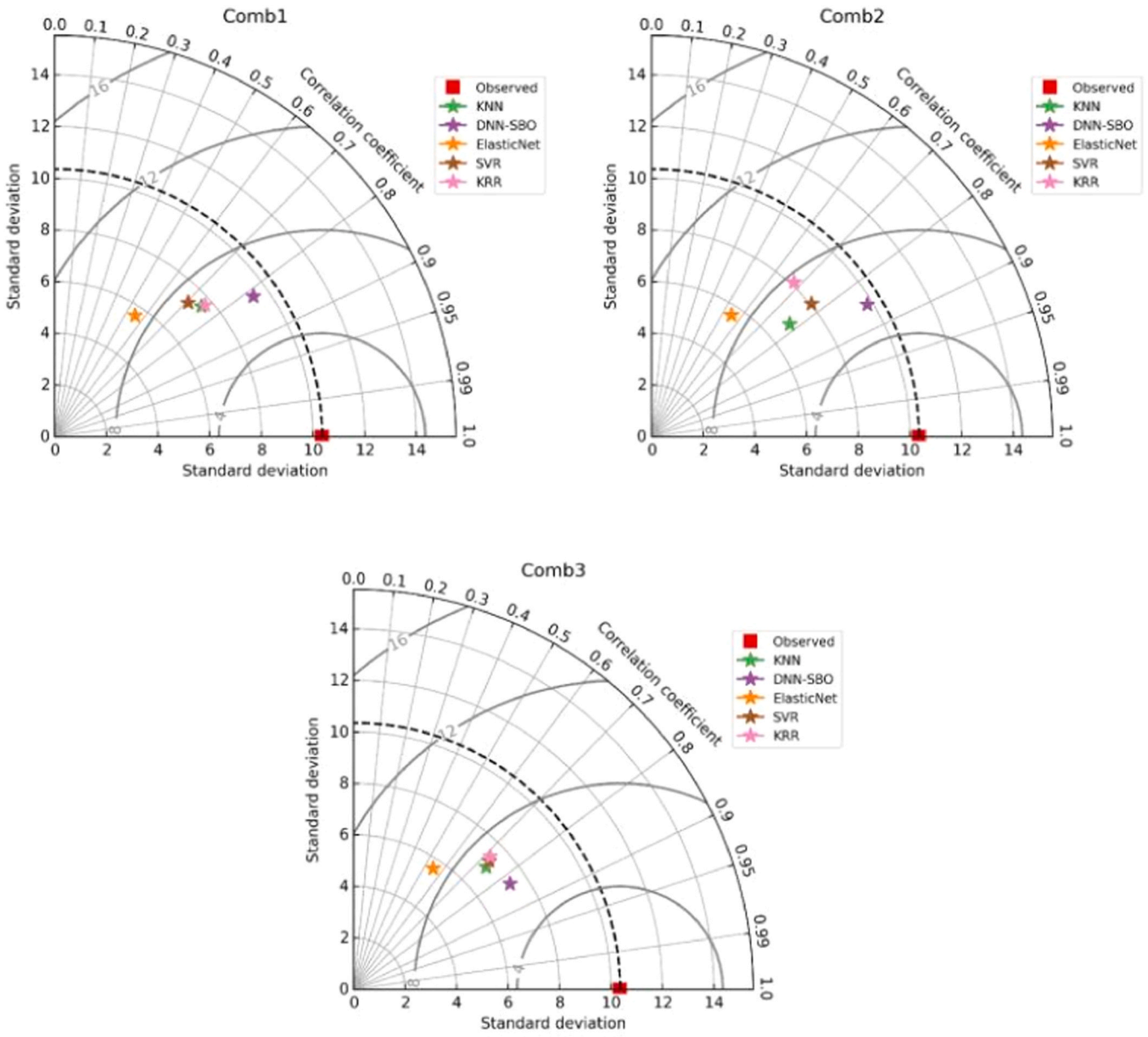

Fig. 9. Taylor Diagrams for different scenarios.

decrease in yield (Fageria et al., 2008). Iron is the most critical micronutrient, necessitating increased quantities for the metabolic processes of plants. Iron is a significant component of various compounds and enzymes, and it also aids in the reduction of nitrate and sulfate. The plant body's energy production is significantly influenced by iron. Chlorophyll synthesis is one of the most essential functions of iron. This is the cause of the chlorosis observed in juvenile, new foliage in iron-deficient environments. Iron is a critical component of numerous enzymatic systems, including peroxidases, cytochromes, and catalases. These systems utilize heme as a prosthetic group, with cytochrome being particularly essential in the regulation of the respiratory system (Mushtaq et al., 2025).

4.4. Limitations

Nevertheless, there are definite limitations to the described research. First, it should be noted that focusing on soil variables, seasonal variations in rainfall, temperature extremes, and disease pressure are not considered; this fact may decrease the generalizability or hide important weather-related trends. Second, despite the fact that close to 600 field measurements in two growing seasons are a large dataset to use as field-sampling standards, deep neural networks can be trained on even more datasets to prevent overfitting. Third, the multi-stage method used by the authors might require a significant amount of computation, particularly when the data scale increases or when real-time forecasting of the farm is required. Lastly, similar to most deep-learning solutions, DNNs may be black box making them unhelpful to stakeholders seeking explanations, although the paper has sought to address this aspect by introducing SHAP analysis to attribute features to them.

4.5. Future research recommendations

On the one hand, further research may consider a wider range of environmental conditions (such as daily temperatures, precipitation, pest occurrence) or remote-sensing data to show a more comprehensive perspective of yield variability. The data-augmentation approaches (combining years/worksites or using several types of satellite images) are also likely to improve the strength of the model. To gain further

Table 2
– Results of uncertainty analysis.

Model	AE	SD	SE	ME	LB	UB	WCB
KNN-C1	5.322	6.905	0.630	1.235	45.499	47.970	2.471
DNN-SBO-C1	**4.804**	**6.063**	**0.553**	**1.085**	**45.654**	**47.824**	**2.170**
Elastic Net-C1	6.920	8.670	0.791	1.551	45.444	48.546	3.103
SVR-C1	5.665	7.367	0.673	1.318	45.933	48.570	2.636
KRR-C1	5.459	6.844	0.625	1.224	45.862	48.311	2.449
KNN-C2	5.358	6.661	0.608	1.192	45.759	48.143	2.384
DNN-SBO-C2	**4.393**	**5.505**	**0.503**	**0.985**	**44.772**	**46.742**	**1.970**
Elastic Net-C2	6.958	8.689	0.793	1.555	45.425	48.534	3.109
SVR-C2	5.007	6.640	0.606	1.188	45.568	47.944	2.376
KRR-C2	5.964	7.709	0.704	1.379	45.208	47.967	2.759
KNN-C3	5.745	7.072	0.646	1.265	46.160	48.691	2.531
DNN-SBO-C3	**4.841**	**5.940**	**0.542**	**1.063**	**44.973**	**47.098**	**2.125**
Elastic Net-C3	6.927	8.680	0.792	1.553	45.436	48.542	3.106
SVR-C3	5.581	7.139	0.652	1.277	46.169	48.724	2.554
KRR-C3	5.779	7.252	0.662	1.297	45.668	48.263	2.595

understanding of model uncertainty, frameworks that are based on Bayesian model or bootstrap ensembles might be used to better measure predictive reliability. Lastly, it may be prudent to verify the proposed DNN-SBO scheme in other potato-growing areas or on other crops (e.g., wheat, rice, maize) to understand the extent to which the approach is applicable to other agronomic settings. In general, the paper does an excellent job at generalizing yield-forecasting methods based on a highly sophisticated and soil-focused ML approach, yet a more comprehensive data paradigm and comprehensive cross-regional testing would also help the paper to cement its practical usefulness.

5. Conclusion

This study proposed a novel hybrid machine learning method using soil properties and characteristics, i.e., DNN-SBO, for predicting potato yields across eight sites in New Brunswick and Prince Edward Island, Canada, using soil properties. The framework combines Boruta feature selection, Best Subset Regression, and the WASPAS method to identify the most influential input variables, while Satin Bowerbird Optimization (SBO) is used to fine-tune DNN hyperparameters. Among three input scenarios, Comb2 (comprising Total Base Saturation, Sulfur,

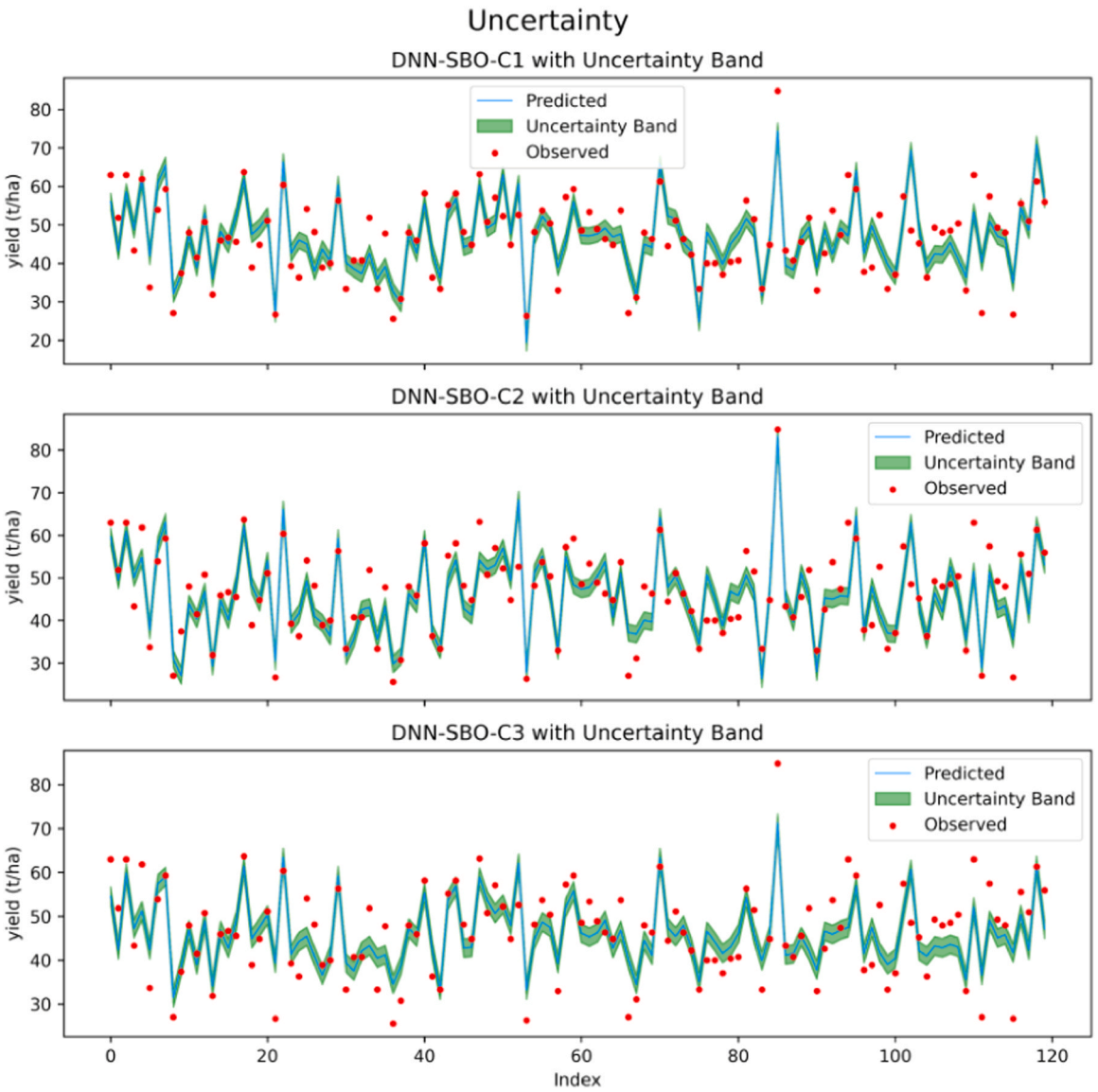

Fig. 10. – Uncertainty Interval plots for the superior model in three scenarios.

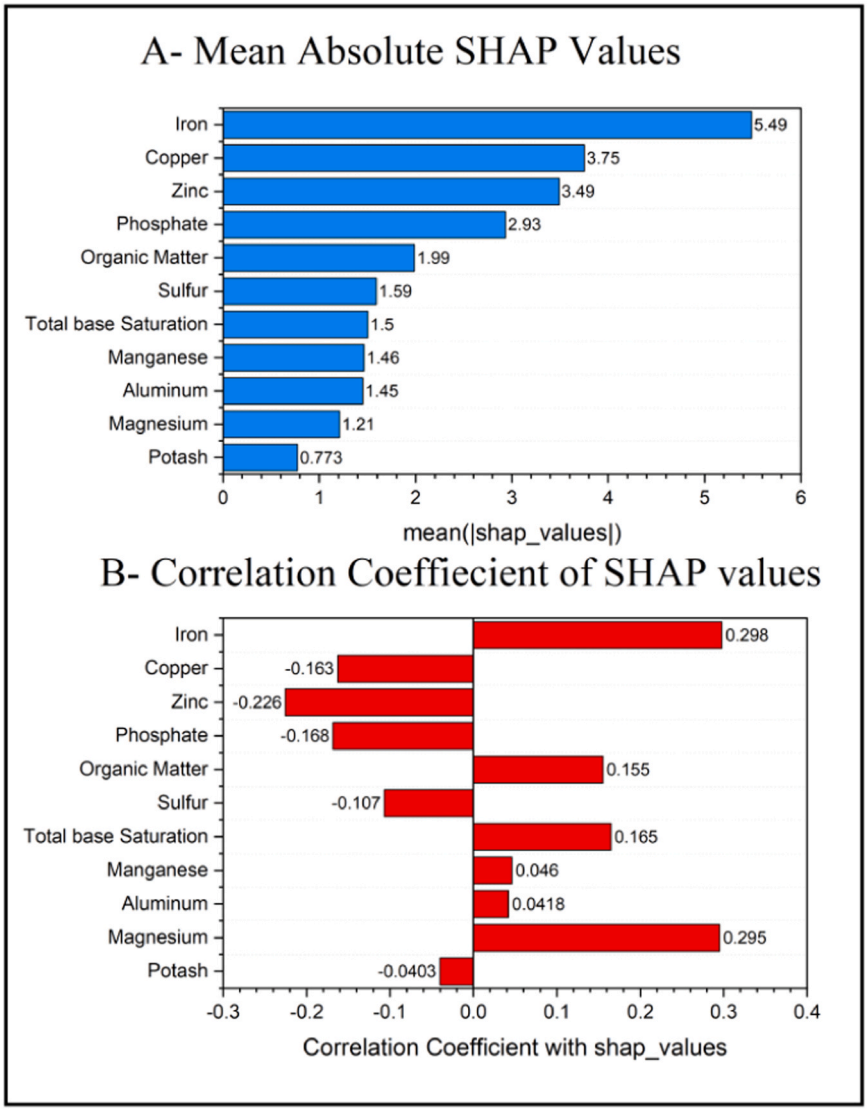

Fig. 11. Bar Plots of SHAP analysis for global interpretation.

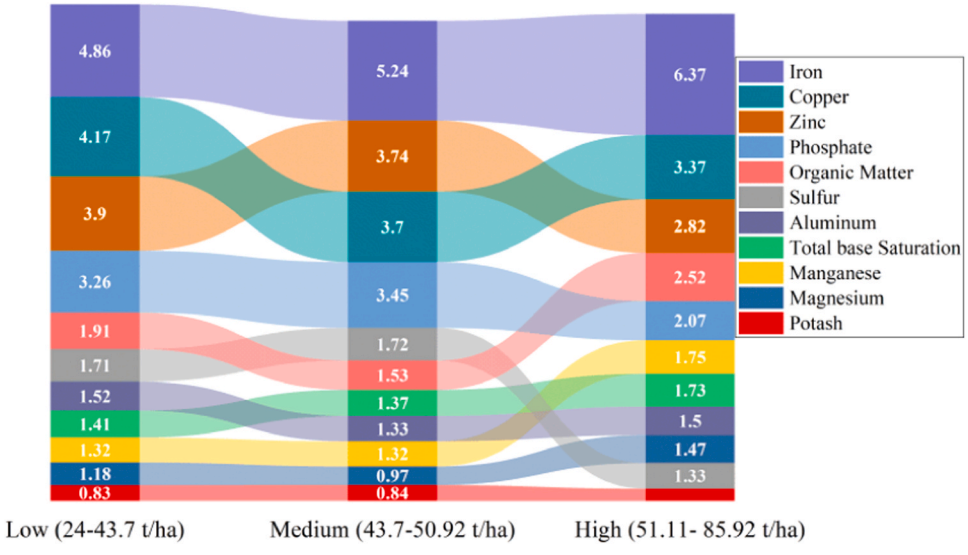

Fig. 12. SHAP summary plots for different ranges of potato yield.

Magnesium, Potash, Aluminum, Zinc, Phosphate, Manganese, Organic Matter, Iron, and Copper) produced the highest accuracy, with R = 0.853 and RMSE = 5.522 t/ha during testing. Comparative models (KRR, Elastic Net, KNN, SVR) were outperformed by the DNN-SBO across all evaluation metrics. SHAP analysis also increased the interpretability of the model and Iron was the most influential feature followed by Copper, Zinc, Phosphorus, and Organic Matter. Such results corroborate the idea that the suggested DNN-SBO framework can capture complicated nonlinear relationships between the characteristics of soil and yield. Further research ought to incorporate more environmental variables like the irrigation level, the occurrence of pests, and weather information and test the model over other areas and crop varieties to reinforce its use in precision agriculture. Comprehensively, the study will add a strong and interpretable yield forecasting system that would support the sustainable agriculture in the Canadian Maritime provinces as a response to soil variability.

Funding

This work has been supported by the Natural Sciences and Engineering Research Council of Canada (NSERC) Discovery Grants [RGPIN-2022–03547 to G.S.R. and RGPIN-2023–03351 to A.A.F.] and NSERC Alliance Sustainable Agriculture Research Initiative Grant [ALLRP 588581 – 23 to A.A.F.]. The authors would like to thank the participating growers, project partners, and collaborators for their support in this research study. Sincere gratitude to the Sustainable Agriculture Research Group at the University of Prince Edward Island for their assistance during data collection.

CRediT authorship contribution statement

Qamar U. Zaman: Writing – review & editing, Validation, Supervision, Project administration. **Anurag Malik:** Writing – review & editing, Visualization, Validation, Formal analysis. **Aitazaz A. Farooque:** Writing – review & editing, Validation, Project administration, Investigation, Funding acquisition. **Gurjit S. Randhawa:** Writing – review & editing, Validation, Supervision, Funding acquisition, Formal analysis. **Masoud Karbasi:** Writing – review & editing, Writing – original draft, Visualization, Software, Methodology, Investigation, Formal analysis, Data curation, Conceptualization. **Hassan Afzal:** Writing – review & editing, Visualization, Software, Investigation. **Khabat Khosravi:** Writing – review & editing, Validation, Methodology, Formal analysis. **Mehdi Jamei:** Writing – review & editing, Validation, Methodology, Investigation, Formal analysis. **Mumtaz Ali:** Writing – review & editing, Visualization, Supervision, Investigation.

Declaration of Competing Interest

The authors declare that they have no known competing financial interests or personal relationships that could have appeared to influence the work reported in this paper.

Appendix A. Supporting information

Supplementary data associated with this article can be found in the online version at doi:10.1016/j.fcr.2025.110311.

Data availability

The authors do not have permission to share data.

References

Abrougui, K., Gabsi, K., Mercatoris, B., Khemis, C., Amami, R., Chehaibi, S., 2019. Prediction of organic potato yield using tillage systems and soil properties by artificial neural network (ANN) and multiple linear regressions (MLR). Soil Tillage Res. 190, 202–208.

Akaike, H., 1974. A new look at the statistical model identification. IEEE Trans. Autom. Contr. 19, 716–723.

Al-Jawarneh, A.S., Ismail, M.T., Awajan, A.M., 2021. Elastic net regression and empirical mode decomposition for enhancing the accuracy of the model selection. Int. J. Math. Eng. Manag. Sci. 6, 564–583. https://doi.org/10.33889/IJMEMS.2021.6.2.034.

Altman, N.S., 1992. An introduction to kernel and nearest-neighbor nonparametric regression. Am. Stat. 46, 175–185.

Bindraban, P.S., van der Velde, M., Ye, L., Van den Berg, M., Materechera, S., Kiba, D.I., Tamene, L., Ragnarsdóttir, K.V., Jongschaap, R., Hoogmoed, M., 2012. Assessing the impact of soil degradation on food production. Curr. Opin. Environ. Sustain. 4, 478–488.

Bowman, R.A., Olsen, S.R., Watanabe, F.S., 1978. Greenhouse evaluation of residual phosphate by four phosphorus methods in neutral and calcareous soils. Soil Sci. Soc. Am. J. 42, 451–454.

Brown, J.R., Cisco, J.R., 1984. An improved Woodruff buffer for estimation of lime requirements. Soil Sci. Soc. Am. J. 48, 587–592.

Cao, J., Zhang, Z., Luo, Y., Zhang, L., Zhang, J., Li, Z., Tao, F., 2021a. Wheat yield predictions at a county and field scale with deep learning, machine learning, and google earth engine. Eur. J. Agron. 123, 126204.

Cao, J., Zhang, Z., Tao, F., Zhang, L., Luo, Y., Zhang, J., Han, J., Xie, J., 2021b. Integrating multi-source data for rice yield prediction across China using machine learning and deep learning approaches. Agric. For. Meteor. 297, 108275.

Chellamani, G.K., Chandramani, P.V., 2020. An optimized methodical energy management system for residential consumers considering price-driven demand response using satin bowerbird optimization. J. Electr. Eng. Technol. 15, 955–967. https://doi.org/10.1007/s42835-019-00338-z.

Chen, W., Chen, X., Peng, J., Panahi, M., Lee, S., 2021. Landslide susceptibility modeling based on ANFIS with teaching-learning-based optimization and Satin bowerbird optimizer. Geosci. Front. 12, 93–107. https://doi.org/10.1016/j.gsf.2020.07.012.

Chintam, J., Daniel, M., 2018. Real-power rescheduling of generators for congestion management using a novel Satin Bowerbird optimization algorithm. Energies 11, 183. https://doi.org/10.3390/en11010183.

Conijn, J.G., Bindraban, P.S., Schröder, J.J., Jongschaap, R.E.E., 2018. Can our global food system meet food demand within planetary boundaries? Agric. Ecosyst. Environ. 251, 244–256.

Debnath, B., Bari, A.B.M.M., Haq, M.M., de Jesus Pacheco, D.A., Khan, M.A., 2023. An integrated stepwise weight assessment ratio analysis and weighted aggregated sum product assessment framework for sustainable supplier selection in the healthcare supply chains. Supply Chain Anal. 1, 100001.

Dikshit, A., Pradhan, B., 2021. Interpretable and explainable AI (XAI) model for spatial drought prediction. Sci. Total Environ. 801, 149797. https://doi.org/10.1016/j.scitotenv.2021.149797.

Eed, M., Alhussan, A.A., Qenawy, A.-S.T., Osman, A.M., Elshewey, A.M., Arnous, R., 2024. Potato consumption forecasting based on a hybrid stacked deep learning model. Potato Res. 1–25.

El Bilali, A., Abdeslam, T., Ayoub, N., Lamane, H., Ezzaouini, M.A., Elbeltagi, A., 2023. An interpretable machine learning approach based on DNN, SVR, Extra Tree, and XGBoost models for predicting daily pan evaporation. J. Environ. Manag. 327, 116890.

El-Kenawy, E.-S.M., Alhussan, A.A., Khodadadi, N., Mirjalili, S., Eid, M.M., 2024. Predicting potato crop yield with machine learning and deep learning for sustainable agriculture. Potato Res. 1–34.

Fageria, N.K., Baligar, V.C., Li, Y.C., 2008. The role of nutrient efficient plants in improving crop yields in the twenty first century. J. Plant Nutr. 31, 1121–1157.

Fan, Y., Liu, Y., Yue, J., Jin, X., Chen, R., Bian, M., Ma, Y., Yang, G., Feng, H., 2024. Estimation of potato yield using a semi-mechanistic model developed by proximal remote sensing and environmental variables. Comput. Electron. Agric. 223, 109117.

Gupta, H.V., Kling, H., Yilmaz, K.K., Martinez, G.F., 2009. Decomposition of the mean squared error and NSE performance criteria: implications for improving hydrological modelling. J. Hydrol. 377, 80–91.

Haws, D.C., Rish, I., Teyssedre, S., He, D., Lozano, A.C., Kambadur, P., Karaman, Z., Parida, L., 2015. Variable-selection emerges on top in empirical comparison of whole-genome complex-trait prediction methods. PLOS One 10, e0138903. https://doi.org/10.1371/journal.pone.0138903.

Hendershot, W.H., Duquette, M., 1986. A simple barium chloride method for determining cation exchange capacity and exchangeable cations. Soil Sci. Soc. Am. J. 50, 605–608.

Jamei, M., Ali, M., Karbasi, M., Karimi, B., Jahannemaei, N., Farooque, A.A., Yaseen, Z. M., 2024. Monthly sodium adsorption ratio forecasting in rivers using a dual interpretable glass-box complementary intelligent system: hybridization of ensemble TVF-EMD-VMD, Boruta-SHAP, and eXplainable GPR. Expert Syst. Appl. 237, 121512.

Jangid, A.K., Khatti, J., Grover, K.S., 2025. Effect of multicollinearity in assessing the compaction and strength parameters of lime-treated expansive soil using artificial intelligence techniques. Multiscale Multidiscip. Model. Exp. Des. 8, 68.

Jayne, T.S., Sanchez, P.A., 2021. Agricultural productivity must improve in sub-Saharan Africa. Science 372 (80), 1045–1047.

Jia, F., Zhu, Z., Dai, W., Le, V.V., 2024. Short-term forecasting of streamflow by integrating machine learning methods combined with metaheuristic algorithms. Expert Syst. Appl. 245, 123076.

Jović, A., Brkić, K., Bogunović, N., 2015. A review of feature selection methods with applications. Proceedings of the 2015 38th International Convention on Information and Communication Technology, Electronics and Microelectronics (MIPRO). IEEE, pp. 1200–1205.

Karbasi, M., Ali, M., Bateni, S.M., Jun, C., Jamei, M., Yaseen, Z.M., 2024. Boruta extra tree-bidirectional long short-term memory model development for Pan evaporation forecasting: investigation of arid climate condition. Alex. Eng. J. 86, 425–442.
Kellner, L., Stender, M., Polach, F. von B. und, Ehlers, S., 2022. Predicting compressive strength and behavior of ice and analyzing feature importance with explainable machine learning models. Ocean Eng. 255, 111396. https://doi.org/10.1016/j.oceaneng.2022.111396.
Kobayashi, M., Sakata, S., 1990. Mallows' Cp criterion and unbiasedness of model selection. J. Econ. 45, 385–395.
Kuradusenge, M., Hitimana, E., Hanyurwimfura, D., Rukundo, P., Mtonga, K., Mukasine, A., Uwitonze, C., Ngabonziza, J., Uwamahoro, A., 2023. Crop yield prediction using machine learning models: case of Irish potato and maize. Agriculture 13, 225.
Kurek, J., Niedbała, G., Wojciechowski, T., Świderski, B., Antoniuk, I., Piekutowska, M., Kruk, M., Bobran, K., 2023. Prediction of potato (Solanum tuberosum L.) yield based on machine learning methods. Agriculture 13, 2259.
Kursa, M.B., Rudnicki, W.R., 2010. Feature selection with the Boruta package. J. Stat. Softw. 36, 1–13.
Li, D., Miao, Y., Gupta, S.K., Rosen, C.J., Yuan, F., Wang, C., Wang, L., Huang, Y., 2021. Improving potato yield prediction by combining cultivar information and UAV remote sensing data using machine learning. Remote Sens. 13, 3322.
Liu, W., Li, Q., 2017. An efficient elastic net with regression coefficients method for variable selection of spectrum data. PLOS One 12, e0171122. https://doi.org/10.1371/journal.pone.0171122.
Liu, Y., Liang, Y., 2024. Satin bowerbird optimizer-neural network for approximating the capacity of CFST columns under compression. Sci. Rep. 14, 8342. https://doi.org/10.1038/s41598-024-58756-7.
Lotze-Campen, H., Müller, C., Bondeau, A., Rost, S., Popp, A., Lucht, W., 2008. Global food demand, productivity growth, and the scarcity of land and water resources: a spatially explicit mathematical programming approach. Agric. Econ. 39, 325–338.
Marschner, H., 2011. Marschner's mineral nutrition of higher plants. Academic press.
Mayer, K.D., Starkey, B.J., 1977. Simpler flame photometric determination of erythrocyte sodium and potassium: the reference range for apparently healthy adults. Clin. Chem. 23, 275–278.
Mishra, P., Al Khatib, A.M.G., Mohamad Alshaib, B., Kuamri, B., Tiwari, S., Singh, A.P., Yadav, S., Sharma, D., Kumari, P., 2023. Forecasting potato production in major South Asian countries: a comparative study of machine learning and time series models. Potato Res. 1–19.
Mishra, A.R., Singh, R.K., Motwani, D., 2019. Multi-criteria assessment of cellular mobile telephone service providers using intuitionistic fuzzy WASPAS method with similarity measures. Granul. Comput. 4, 511–529.
Moayedi, H., Mosavi, A., 2021. Electrical power prediction through a combination of multilayer perceptron with water cycle ant lion and satin bowerbird searching optimizers. Sustainability 13, 2336. https://doi.org/10.3390/su13042336.
Molnar, C., 2020. Interpretable Machine Learning. Lulu Press. Morrisville, NC, USA.
Moosavi, S.H.S., Bardsiri, V.K., 2017. Satin bowerbird optimizer: a new optimization algorithm to optimize ANFIS for software development effort estimation. Eng. Appl. Artif. Intell. 60, 1–15. https://doi.org/10.1016/j.engappai.2017.01.006.
Muruganantham, P., Wibowo, S., Grandhi, S., Samrat, N.H., Islam, N., 2022. A systematic literature review on crop yield prediction with deep learning and remote sensing. Remote Sens. 14, 1990.
Mushtaq, Z., Alasmari, A., Demir, C., Oral, M.A., Bellitürk, K., Baran, M.F., 2025. Enhancing iron content in potatoes: a critical strategy for combating nutritional deficiencies. Potato Res. 68, 715–741.
Narisetty, N.N., 2020. Bayesian model selection for high-dimensional data. pp. 207–248. ⟨https://doi.org/10.1016/bs.host.2019.08.001⟩.
Naskath, J., Sivakamasundari, G., Begum, A.A.S., 2023. A study on different deep learning algorithms used in deep neural nets: MLP SOM and DBN. Wirel. Pers. Commun. 128, 2913–2936. https://doi.org/10.1007/s11277-022-10079-4.
Organization, W.H., 2021. World hunger is still not going down after three years and obesity is still growing—UN report. 2019.
Paudel, D., Boogaard, H., de Wit, A., Janssen, S., Osinga, S., Pylianidis, C., Athanasiadis, I.N., 2021. Machine learning for large-scale crop yield forecasting. Agric. Syst. 187, 103016.
Pedregosa, F., Varoquaux, G., Gramfort, A., Michel, V., Thirion, B., Grisel, O., Blondel, M., Prettenhofer, P., Weiss, R., Dubourg, V., 2011. Scikit-learn: machine learning in Python. J. Mach. Learn. Res. 12, 2825–2830.
Piekutowska, M., Niedbała, G., 2025. Review of methods and models for potato yield prediction. Agriculture 15, 367.
Ravindran, S.M., Bhaskaran, S.K.M., Ambat, S.K.N., 2021. A deep neural network architecture to model reference evapotranspiration using a single input meteorological parameter. Environ. Process 8, 1567–1599. https://doi.org/10.1007/s40710-021-00543-x.
Rezaei, I., Amirshahi, S.H., Mahbadi, A.A., 2023. Utilizing support vector and kernel ridge regression methods in spectral reconstruction. Results Opt. 11, 100405.
Rijsberman, F.R., Molden, D., 2001. Balancing water uses: Water for food and water for nature, in: Thematic Background Paper to the International Conference on Freshwater, Bonn. pp. 43–56..
Roger-Estrade, J., Richard, G., Boizard, H., Boiffin, J., Caneill, J., Manichon, H., 2000. Modelling structural changes in tilled topsoil over time as a function of cropping systems. Eur. J. Soil Sci. 51, 455–474.
Schulte, E.E., Hopkins, B.G., 1996. Estimation of soil organic matter by weight loss-on-ignition. Soil Org. Matter Anal. Interpret 46, 21–31.
Seyyedabbasi, A., Aliyev, R., Kiani, F., Gulle, M.U., Basyildiz, H., Shah, M.A., 2021. Hybrid algorithms based on combining reinforcement learning and metaheuristic methods to solve global optimization problems. Knowl. Based Syst. 223, 107044.
Shapley, L.S., 1953. A value for n-person games, In: Proceedings of the Contributions to the Theory of Games (AM-28), Volume II. Princeton University Press, pp. 307–318. https://doi.org/10.1515/9781400881970-018.
Shen, C., 2018. A transdisciplinary review of deep learning research and its relevance for water resources scientists. Water Resour. Res. 54, 8558–8593. https://doi.org/10.1029/2018WR022643.
Subasi, A., 2020. Machine learning techniques. Proceedings of the Practical Machine Learning for Data Analysis Using Python. Elsevier, pp. 91–202. https://doi.org/10.1016/B978-0-12-821379-7.00003-5.
Subramaniam, L.K., Marimuthu, R., 2024. Crop yield prediction using effective deep learning and dimensionality reduction approaches for Indian regional crops. ePrimeAdv. Electr. Eng. Electron. Energy 8, 100611.
Tamayo-Vera, D., Liu, K., Bolufé-Röhler, A., Wang, X., 2024. Projecting future changes in potato yield using machine learning techniques: a case study for Prince Edward Island, Canada. Environ. Res. Commun. 6, 105025.
Tamayo-Vera, D., Mesbah, M., Zhang, Y., Wang, X., 2025. Advanced machine learning for regional potato yield prediction: analysis of essential drivers. npj Sustain. Agric. 3, 12.
Utama, C., Meske, C., Schneider, J., Schlatmann, R., Ulbrich, C., 2023. Explainable artificial intelligence for photovoltaic fault detection: a comparison of instruments. Sol. Energy 249, 139–151. https://doi.org/10.1016/j.solener.2022.11.018.
Van Klompenburg, T., Kassahun, A., Catal, C., 2020. Crop yield prediction using machine learning: a systematic literature review. Comput. Electron. Agric. 177, 105709.
Vapnik, V., Golowich, S., Smola, A., 1996. Support vector method for function approximation, regression estimation and signal processing. Adv. Neural Inf. Process. Syst. 9.
Wilson, A.D., 1960. The micro-determination of ferrous iron in silicate minerals by a volumetric and a colorimetric method. Analyst 85, 823–827.
Zavadskas, E.K., Turskis, Z., Antucheviciene, J., Zakarevicius, A., 2012. Optimization of weighted aggregated sum product assessment. Elektron. Ir. Elektro 122 (6), 3.
Zhu, X., Li, J., Zhu, M., Jiang, Z., Li, Y., 2018. An evaporation duct height prediction method based on deep learning. IEEE Geosci. Remote Sens. Lett. 15, 1307–1311. https://doi.org/10.1109/LGRS.2018.2842235.
Zou, H., Hastie, T., 2005. Regularization and variable selection via the elastic net. J. R. Stat. Soc. Ser. B Stat. Method. 67, 301–320. https://doi.org/10.1111/j.1467-9868.2005.00503.x.